

FINAL REPORT

1. Project Title: <i>Encapsulation and controlled delivery of herbal extracts in dairy food matrix using cow milk protein against in vitro simulated inflammatory cell line models.</i>	DST No: SB/YS/LS-30/2014
2. PI (Name & Address): Dr. Raj Kumar Duary, Assistant Professor, Department of Food Engineering and Technology, School of Engineering , Tezpur University (Central University), Napaam, Sonitpur, Assam, INDIA-784 028. Telephone: +91-3712-275709 Fax: +91-3712-267005 E-mail: rkduary@gmail.com	Date of Birth 01-06-1982
3. Co-PI (Name & Address): NIL	Date of Birth: NA
4. Broad area of Research: Life Science 4.1 Sub Area Agricultural Science 5. Approved Objectives of the Proposal : <ul style="list-style-type: none"> ➤ Collection of the medicinal plants different sources; standardization of extraction processes and biochemical characterization (total phenolic compounds, flavonoid content, anti-oxidative properties, etc) of the extracts. ➤ Study the efficiency of the plant extracts to block inflammation in cell culture model. ➤ To encapsulate the extracts using milk proteins in nano-beads and use it to supplement in a food matrix. ➤ Incorporating Nanocomposites in a suitable food/dairy matrix as a carrying vehicle. 	
Date of Start: 10/October/2014	Total cost of Project: Rs. 19.70 lakhs Received Fund: Rs. 16.00 lakhs
Date of completion: March, 2017	Expenditure as on 31.03.2017: Rs. 16.00075 lakhs
6. Methodology : <ul style="list-style-type: none"> ➤ For studying biomolecule functionality and establishing their functional potentiality: Collection of the medicinal plants different sources; standardization of extraction processes and biochemical characterization (total phenolic compounds, flavonoid content, anti-oxidative properties, etc) of the extracts. ➤ Study the efficiency of the plant extracts to block inflammation in cell culture model. ➤ To encapsulate the extracts using milk proteins in nano-beads and use it to supplement in a food matrix. 	

6.1. *In silico* identification of natural biomolecules as selective ADAM17 inhibitors.

6.1.1. PDB entries used in search and docking

The three-dimensional crystal structure of ADAM17 (PDB ID: 2IO0) determined by X-ray crystallography was retrieved from the Protein Databank Bank (<http://www.rcsb.org/>) was imported into the CLC (Qaigen). Figure 1 shows the protein ADAM17 and its active site. The crystal structures 1HFC for MMP1, 3AYU for MMP2, 1HY7 for MMP3, 2Y6D for MMP7, 1I76 for MMP8, 2OVX for MMP9, 3ZHX for MMP13, and 1RM8 for MMP16 were used to sort out the selectivity problem. The coordinates of the di/tri/quadameric crystallographic structure were complexed with water molecules. Considering that the monomers are identical and independent of each other, only monomer A from the enzyme, were selected to perform the molecular docking studies. This procedure reduced the computation time by half. The co-crystallized water molecules and ligands were removed from both the monomers.

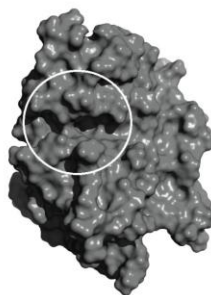


Figure 1: ADAM17 surface structure and the active site cavity marked by white circle.

6.1.2. High throughput virtual screening

32 compounds which are known to have the potential to down regulate inflammatory bowel diseases were used for this study. These compounds were already established as possible inhibitors of inflammation pathways on animal and cell line models. The 3D structures of compounds were retrieved from the NCBI PubChem database. No energy minimization was performed as ligand torsions were set free and subjected to flexible docking.

For the purposes of this study, prior filtering using the ‘rule-of five’ served to remove a variety of compounds, which are either likely to be poorly absorbed, or else are likely to undergo extensive modification prior to absorption. This was the first filter used to screen these potential leads.

A well-known optimized compound IK-682 was added to the database as a reference molecule. As there is a selectivity issue with ADAM17 inhibitors because of MMPs having similar catalytic site as that of ADAM17, ADAM17 inhibitors bind with MMPs also.

For docking purposes, the co-crystallized ligands were used to predict binding site and set as search space centers. The active site residues of proteins were predicted from available literature and uniProt database.



Figure 2: Figure showing the active site search space for ADAMI7 (2OI0).

The active site residues were set in the search space (Figure 2) inside a restriction sphere of radius 13 Å. The docking algorithm was set at a maximum iteration of 500 and run with virtual ligand screening mode. Ligand torsions were set free and docking was performed with a limit of five retained poses per molecule. For each compound the lowest energy pose was then selected from these five solutions.

In order to assess the efficacy of CLC Drug discovery workbench 2.4 in finding low energy solutions for those PDB entries included in this study, crystal ligands were also docked to their respective receptors, the top ranking score recorded, and the RMSD of that pose from the corresponding crystal co-ordinates computed. Docking studies were visualized in CLC or PyMol, and were performed at Intel(R) Core(TM) i3 CPU (3.20 GHz) with Microsoft Windows 7.

6.1.3. ADMET

ADMETsar were used for assessing the disposition and potential toxicity of a ligand within an organism. Human Intestinal Absorption (HIA) was predicted so that oral delivery was identified by using drug based models for *in vitro* Caco2-cell assay. Also (BBB) blood brain barrier penetration of therapeutic drug in the central nervous system (CNS) was identified. Simultaneously, mutagenicity by Ames TA 100, Ames TA 1535, Ames TA 98 and Carcinogenicity in rats and mouse were detected.

6.1.4. Molecular dynamic simulations

The simulations were performed using a Gromacs package 4.5.0. The visualization of snapshots and trajectories at different time frames during the course of dynamics simulation was projected using visual molecular dynamics and PyMOL packages to get a pictorial depiction of the interaction. MD simulations were performed on Ubuntu14.0 Linux operating system in a Intel(R) Core(TM) i7 CPU 3.20 GHz at the Bioinformatics Facility at the Department of Molecular Biology and Biotechnology, Tezpur University, India.

6.2. Screening, Extraction and Purification of natural biomolecule from locally available medicinal plants.

6.2.1 Sample Preparation and Chemicals

Capsicum chinense (Bhut Jolokiya) fruit dry powder from Golaghat district of Assam, India. The powder was sun dried for a day, ground, sieved through 20–30 mesh and kept in air tight containers placed inside desiccators until further process.

M. Olifera (Sajana) and *Polygonum microcephalum* (Madhu-soleng) leaves were collected from local household in Napaam, Tezpur, Assam, a northeastern state of India. Fresh leaves were dried in a Cross flow tray drier at $50\pm 5^{\circ}\text{C}$ for 24 hour. Dried leaves were crushed and powdered in a mixer grinder (Philips, India) were then placed inside a desiccators until further process.

The standard Quercetin was purchased from Sigma Chemical Co, St. Louis, MO, USA. All HPLC solvents used for flavonoid analysis were of HPLC grade from Merck (India). All other chemicals used in the experimentation procedure were of analytical grade purchased from Merck. Water used in all the experiments was double distilled and deionised (Elix Millipore Water Purification System, USA). All solutions were filtered through $0.22\mu\text{m}$ cellulose-nitrate membrane filters (HiMedia Labs, India) before HPLC injection and the mobile phase solvents were degassed before use using 20 minutes of sonication in a waterbath sonicator.

6.2.2. Estimation of Total Flavanoids

The aluminum chloride method was used for the determination of the total flavonoid content of the extracts (Far et al., 2009). The concentrations of flavonoid in the test samples were calculated from the calibration plot and expressed as mg quercetin equivalent /g of sample.

6.2.3. Experimental Design and Optimization

A three-variable, three-level Box–Behnkem design (BBD) (Simsek et al., 2012) was applied to determine the best combination of extraction variables for the yield of Quercetin from *Capsicum chinense* (Bhut Jolokiya) fruit. The three independent variables set were solvent concentration (% , X_1), irradiation time (min, X_2) and acidification (% , X_3), and each variable set at three levels. The independent variables were coded at three levels and their actual values selected on the basis of preliminary experimental results. The coded and uncoded (actual) levels of the independent variables are given in Table 1. Experiments were augmented with 5 replications at the centre point to evaluate the pure error. RSM was applied to the experimental data using a commercial statistical package, Design-Expert version 6.0.11 (Stat-Ease, Inc., Minneapolis, MN, USA). The same software was used for the generation of response surface plots, superimposition of contour plots and optimization of process variables.

Table 1. Code level of factors trials.	Factor	Low -	Center 0	High +	and uncoded chosen for the
	Solvent concentration (% , X_1)	-1 (50)	0 (75)	1 (100)	
	Acidification (% , X_2)	-1 (1)	0 (1.5)	1 (2)	
	Irradiation time (min, X_3)	-1 (2)	0 (5)	1 (8)	

The experiments were conducted randomly to minimize the effects of unexplained variability in the observed responses as a result of external factors (Jokic *et al.* 2007). Regression analysis for the experiment data was performed, and was fitted into the empirical second order polynomial model,

$$Y = a_0 + \sum_{i=1}^n a_i x_i + \sum_{i=1}^{n-1} \sum_{j=i+1}^n a_{ij} x_i x_j + \sum_{i=1}^n a_{ii} x_i^2$$

Where Y represents the response variables, a_0 is a constant, a_i , a_{ii} and a_{ij} are the linear, quadratic and interactive coefficients, respectively. X_i and X_j are the levels of the independent variables i and j . Model adequacy was evaluated using F ratio and coefficient of determination (R^2) represented at 1, 5 and 10% level of significance accordingly.

6.2.4. Microwave assisted acid hydrolysis and extraction

Open vessel extractions were carried out in a domestic microwave oven (Samsung Oven, 50 KHz, 1250Watts, India). Powder of 5.0 g dried Capsicum chinense (Bhut Jolokia) fruit was weighed into a glass flat-bottomed flask, vessels were then sealed using ground stopper with varying solvent concentration (50-100%). The samples were kept at room temperature for 90 minutes for leaching of the solvent into the sample (Hong *et al.* 2001). The solvent sample mixture was then acidified (1-2%) using 12 M HCl. and then microwave-irradiated on a carousel for defined time (2–8 mins.). After microwave irradiation, the residues were then filtered and stored at 4 degree Celsius.

6.2.5. Fractionation of Flavanoids

A Sep-Pak C18 cartridge (Waters, Milford, MA, USA) was preconditioned for neutral flavonoids by sequentially passing 8 ml of methanol and 4 ml of distilled–deionized water adjusted to pH 7.0. 3 ml of sample adjusted to pH 7.0 with 1 M NaOH, and then loaded into the neutral fractionating Sep Pak C18 columns and then washed with 10 ml of distilled water (pH 7). The effluent was discarded. The adsorbed fraction was eluted using 12 ml methanol, and then

evaporated to dryness under vacuum at 35°Celsius. The residue was redissolved in 3 ml of methanol, filtered and 15 µl was injected onto the HPLC system. 3 ml standard quercetin solution at 100 ppm was also fractionated as control to estimate column yield (%) (Chen et al., 2001).

6.2.6. RP-HPLC analysis and quantification

The analyses were performed with a Waters HPLC system equipped with a UV-Vis detector. For profiling and quantification, the compounds were separated on a 2.1 X 150 mm Waters reverse phase C18 HPLC column maintained at 30 °C and a mobile phase of (A) 0.1% formic acid in water and (B) 0.1% formic acid in methanol with the following gradient: 10-90% B (0–10 min), 90% B (10-15 min), 90-75% B (15-16 min), 75-55% B (16-20 min), 55-40% B (25–25 min), 40-20% B (25-30 min) 20-10% B (30-35 min) and 10% B (35-45 min) with a flow rate of 0.2 ml/min. All chromatograms were monitored at 280 and 254 nm. Breeze v2.0 software was used to program the gradient and process the chromatographic data. Identification was performed by comparing the retention times of the samples with that of standard. Quantification was made according to the linear calibration curve of standard compound.

6.2.7. Collection of pure fractions from HPLC

Extraction was carried out using the optimized protocol, and fractionated using SPME. The SPME fraction was concentrated 10 folds, and then injected into the RP-HPLC system running at same conditions. Pure fractions were repeatedly collected as they came out the detector. The pool of mobile phase collected containing the biomolecule was freeze dried and biomolecule was recovered as yellow, crystalline powder. Although current purification techniques make use of preparative HPLC systems, because of our instrumental limitation, we had to restrict our collection techniques in this way. However, the technique does not compromise to the consistency of the reported results.

6.2.8. Infrared spectroscopy

The infra-red spectra for the purified compound and standard were obtained with a FTIR spectrometer (PerkinElmer, USA). The equipment was operated with scanning range of 4000–450 cm⁻¹ and spectrum of 100. The fine powder and then sample (clear glassy disk) for FTIR analysis were prepared by mixing powdered sample with IR grade KBr using FTIR hand operated press at around 12,000 psi pressure.

6.2.9. NMR

NMR spectra (¹H and ¹³C spectra) were obtained on a JEOL ECS 400 MHz NMR Spectrometer equipped with multinuclear, direct detection probe, automatic sample changer, variable temperature, and Z-gradient capabilities. Spectra were acquired at 25°C in d₆-DMSO and referenced to residual ¹H signals in the deuterated solvent (δ 2.54).

6.2.10. Cell culture

The human monocytic leukemia cell line THP-1 (American Type Culture Collection, Rockville, Md.) was grown in RPMI 1640 culture medium supplemented with fetal bovine serum (Invitrogen, USA) and penicillin/streptomycin (Invitrogen) to 10% and 1% respectively, at 37°C in 5% CO₂ in a humidified incubator. Cells were sub-cultured twice per week. THP-1 cells change their culture properties after prolonged periods in culture; cells were therefore discarded and replaced by frozen stocks after 25 passages.

6.2.11. Macrophage differentiation and stimulation

The mature macrophage-like state was induced by treating THP-1 monocytes (10⁶ cells ml⁻¹) for 48 h with 100 ng ml⁻¹ phorbol 12-myristate 13-acetate (PMA; Sigma Aldrich, USA) in 6-wells cell culture plates with 1 ml cell suspension in each well. It has been demonstrated that this differentiation method of THP-1 cells resulted in the expression of macrophage specific surface markers CD11b and CD36 and also phagocytic activity. Differentiated, plastic-adherent cells were washed once with sterile phosphate-buffered saline and RPMI 1640 medium without PMA but containing 10% FBS and 1% P/S. Experimental inflammation was induced by treating THP-1 macrophages (differentiated cells) with 1 µg ml⁻¹ LPS, which concentrations were chosen according to our preliminary optimization studies. This was chosen as our positive control. THP-1 cells were stimulated with 100 µM quercetin for 6 hours prior to co-incubation, with and without the presence 1µg ml⁻¹ LPS, for 2 hours. The concentrations of quercetin were chosen according to preliminary optimization studies conducted by Dr. Rupak Mukhopadhyaya, Dept of Molecular Biology and Biotechnology, Tezpur University. THP-1 macrophages without quercetin and without LPS stimulation were chosen as our negative control. All experimental replications were conducted for a total of 8 hours. After stimulation, THP-1 macrophages were harvested at 8 h. Expression of inflammation was determined by quantification of TNF alpha expression on protein level. The experiments were performed by two independent biological replications, started from a new batch of cells.

6.3. Development of colon targeted slow releasing, pH regulated nanocarrier system as biomolecule delivery vehicle.

6.3.1. Purification of Casein.

Casein micelle was purified from fresh cow milk that was collected from a local dairy according to Diaz et al.1996 with slight modifications. The milk was skimmed by centrifugation at 1500g for 30 min at 4 °C. The skimmed milk was stored at 4 °C with 0.05% (w/v) sodium azide to prevent microbial growth if it was not used immediately. Casein proteins were collected by adjusting the pH of milk to 4.6. The pellet that contained casein was then redispersed and washed in Tris buffer (10 mM, pH 7.4) containing 10 mM CaCl₂ for five times to wash out any whey proteins that were loosely adsorbed to casein. We measured the casein content in the solution by the Bradford assay (Bradford 1976) by using bovine serum albumin (BSA) as the standard.

6.3.2. Casein characterization using SDS-PAGE

We carried out SDS-PAGE as described by Laemmli 1970, by using a Bio-Rad mini gel electrophoresis unit. Isolated casein was loaded onto a 12% gel at different concentration and was electrophoresed under a constant current (20 mA). We stained proteins in the gel by using Coomassie Brilliant Blue R-250. The gel was photographed by the use of a gel documentation system (BioRad).

6.3.3. Extraction of starch from waxy rice variety

Waxy rice was collected from local vendor at Nagaon, Assam, India. The rice were washed well with tap water to remove dirt and dried at 30 °C in a tray dryer for two days.

Starch was isolated by a method modified from the methods of Mukprasirt and Sajjaanantakul (2004) and Bobbio et al. (1978).

6.3.4. Preparation of slowly digestible starch products

In brief, 5 g of waxy starch was dispersed with several-fold distilled water and completely gelatinized in boiling water for 30 min. The resulting gels were cooled to 4 °C and subjected to the temperature-cycled retrogradation with different temperature cycles and time intervals for 0–21 days. The retrograded samples were dried at 42 °C for 10 h and milled to pass through a 100-mesh sieve for obtaining the SDS products. Each optimum condition was selected according to the maximum yield of SDS in the products. The following conditions were designed for increasing the SDS yield: temperature cycles (starch to water, 1:3, w/v; at, 4/25 °C, 4/35 °C, 4/45 °C, and 4/55 °C with a time interval of 24 h for 7 d), and temperature-cycled time (starch to water, 1:3, w/v; at the optimum temperature-cycled treatment with a time interval of 24 h for 0, 5, 11, 15, 20, 25 and 30 d).

6.3.5. *In vitro* digestibility determination

In vitro digestibility of the SDS products was measured as a previous procedure described by Englyst et al. 1996. One hundred milligrams of products were used for each measurement. The content of the hydrolyzed starch was calculated by multiplying a factor of 0.9 with the glucose content. The SDS yield and the hydrolysis rate (RH) of the products were obtained as the following equations:

$$\text{SDS (\%)} = 100 \times \left[\frac{(G_{120} - G_{20}) \times 0.9}{\text{Weight of sample}} \right]$$

, where G_{20} is the glucose content released after 20 min, G_{120} is the glucose content released after 120 min. Glucose was measured using the decolorization time of potassium permanganate, and compared with standard glucose decolorization curve.

6.3.6. Scanning electron microscopy (SEM)

Native starch, SDS product produced with the isothermal retrogradation and the optimum temperature-cycled retrogradation, and the SDS product hydrolyzed for 20 min, and 120 min as the previously procedure described in Section 6.3.5 were observed under SEM (JEOL JSM 6390 LV, Singapore).

6.3.7. High pressure Gel Permeation Chromatography

High pressure gel permeation chromatography (HPGPC) was performed using a Waters 2489 system (Millipore, Milford, USA). Starch and SDS product were dissolved in tetrahydrofuran at 100 ppm concentration, and then sonicated for 5 minutes or until dissolve. For the chromatographic separations, a Waters THF HR3 column (Waters Nihon Millipore, USA) was used. Detections were made in RI mode in a RI detector (Waters, Milford, USA). Concentrations of the various fractions were automatically calculated using the EmPower 2.0 data module (Millipore, Milford, USA). THF was used as the mobile phase. The flow rate was 1.0 ml / min.

Sample molecular weight was determined by comparing the area under the elution curve and the total area under the curve of the known polymer standard solution.

6.3.8. Preparation of Conjugates

Casein and SDS with weight ratio of 1:1 were dissolved together in water. The pH of the mixture was adjusted to 8.0 using 1M NaOH, and the solution was lyophilized. The lyophilized powder was reacted at 60°C under 79% relative humidity in a desiccator containing saturated KBr solution for 24 h. The conjugation degree of the resultant Maillard reaction products was analyzed by SDS-PAGE as described by Laemmli 1970, by using a Bio-Rad mini gel electrophoresis unit. Isolated casein was loaded onto a 12% gel at different concentration and was electrophoresed under a constant current (20 mA). We stained proteins in the gel by using Coomassie Brilliant Blue R-250. The gel was photographed by the use of a gel documentation system (BioRad).

6.3.9. Preparation of the blank and loaded Nanocapsules.

As mentioned above, the weight ratio of Casein-SDS was 1:1 in the conjugate preparation. For simplifying the description, we only denote the concentration of Casein in Casein-SDS conjugates. If there is no special indication in this report, the preparation process of the nanocapsules is as follows. The conjugates were dissolved in water and the pH of the mixture was adjusted to 4.6 with 1 M HCl. The mixture was centrifuged at 1000g for 10 mins to pellet out precipitated casein. This step was used as a purification step to remove unconjugated casein. The final suspension was quantified for casein concentration using Bradford assay and then quercetin was added. The final concentration of quercetin to Casein was weight ratio of 1:1. The solution was heated at 80°C for 60 min to produce Quercetin-Casein-SDS nanocapsules. The nanocapsules were further cross-linked using glutaraldehyde. Typically, 5 μ L of 50% glutaraldehyde solution was added in 1 mL of the nanocapsule solution. The cross-linking was

performed under stirring at room temperature for 24 h. The nanocapsule suspension was first at 1000g for 5 minutes, the supernatant collected and recentrifuged at 17000g for 20 mins to collect the Nanocapsules. The pelleted Nanocapsules were redispersed in 1 ml of distilled water and 30mM sucrose solution was added as cryoprotectant at 1:2 w/w (Sucrose: Polymer). The nanocapsule suspension was then lyophilized for 72 hours to obtain powdered Nanocapsules.

Similarly, blank Nanocapsules were also prepared without the addition of quercetin.

6.3.10. Preparation of Transparent Dispersions

To prepare transparent dispersions, 0.25 g of lyophilized powder was hydrated in 20 mL of deionized water for 6 h at room temperature (21 °C) without stirring, then sonicated for three 10 second bursts to obtain the transparent dispersion.

6.3.11. Quercetin Loading Capacity

The unloaded quercetin was separated from the nanocapsules by dialysis technique (cutoff molecular weight of 3.5 MWCO; SnakeSkin™ Dialysis Tubing Thermo Fischer Scientific, USA). The loaded quercetin was calculated by subtracting the free quercetin in the ultrafiltrate from the initial quercetin in feed. Quercetin concentration was determined by its absorbance at 260 nm (Spectronic 20D+, Thermo Scientific, USA) according to the working curve measured using standard quercetin solutions. At least two batches of loading samples were analyzed, and average data were reported.

6.3.12. *In vitro* Quercetin Release

The *in vitro* release profile of quercetin loaded nanocapsules was investigated by dynamic dialysis bag method (Jain et al. 2013) with slight modification. The dialysis bags (cutoff molecular weight of 3.5 MWCO; SnakeSkin™ Dialysis Tubing Thermo Fischer Scientific, USA) were soaked in double-distilled water for 12 h before use. *In vitro* release of Quercetin loaded nanocapsules and free quercetin was carried out in simulated gastric fluids (SGF; pH 2.2, for initial 60 minutes) and simulated intestinal fluids (SIF; pH 6.8). Quercetin loaded nanocapsules and free quercetin equivalent to 2 mg of quercetin were added to dialysis bags, respectively. The release of quercetin was performed in a heated magnetic shaker operated at 37°C at a rate of 100 rpm in 200 mL release medium containing 50% methanol. Samples (2 mL) were withdrawn at predetermined time intervals and replaced with an equal volume of fresh medium each time to maintain the sink condition. The cumulative amount of drug released was analyzed by the UV-Vis method.

The release was quantified as follows:

$$\text{Release (\%)} = (\text{Released quercetin} / \text{total quercetin}) \times 100$$

SGF: NaCl (0.36g), KCl (0.02g), Sodium bicarbonate (0.18g), Pepsin (0.15g) and pH adjusted to

2.2 using 6M HCl in 50ml solutions

SIF: alpha amylase (0.05g), Oxgall bile salts (0.075g), and pH adjusted to 6.8 using 5M NaOH in 50 ml solution.

6.3.13. Nanocapsule surface characteristics

Surface morphology of the loaded and blank nanocapsules was observed under a Scanning Electron Microscope (JEOL JSM 6390 LV, Singapore). Lyophilized samples were sputter coated with platinum and the images were taken at an accelerating voltage of 20 kV and varying magnification.

6.3.14. Thermal properties

The thermal degradation properties of the loaded and blank nanocapsules were determined by Thermo Gravimetric Analysis (TGA). Thermo gravimetric measurement was carried out on a Shimadzu TGA-50 thermogravimetric analyzer. Non-isothermal experiments were performed in the temperature range 25–600°C at heating rates of 10, 20 and 40°C min⁻¹ on each sample. The average sample size was 3 mg and the nitrogen flow-rate was 30 ml min⁻¹.

6.3.15. Dynamic light scattering (DLS) and zeta-potential

The dispersions were diluted 20 times using deionized water and were measured with a Nanotracc wave particle size and Zeta potential analyzer (Microtrac, Angstrom Scientific, NJ, USA) at a scattering angle of 165°. The time correlation functions were analyzed with an inbuilt program to obtain the distribution of the hydrodynamic diameter. The diluted samples at pH 7.0 were also measured for zeta-potential.

6.3.16. UV- Vis Spectroscopic Studies

The quercetin loaded nanocapsules were characterized by absorption spectra. Ranged UV-Vis spectra of 1000 µl of aqueous solution of quercetin, blank nanocapsules and quercetin encapsulated nanocapsules prepared with methanol as co-solvent & blank nanocapsules were recorded on a UV-VIS spectrophotometer (Spectronic 20D+, Thermo Scientific, USA).

6.3.17. Fluorescence Study

Steady-state fluorescence measurements were carried out in a LS 55 Fluorescence spectrometer (Perkin Elmer, USA). Fluorescence spectra of free quercetin, blank nanocapsules and quercetin loaded nanocapsules (methanol as co-solvent) were recorded. An excitation wave-length of 254 and 368 nm with slit widths of 2 nm and scan rate of 1 nm/sec were set as scanning parameters for emission.

6.3.18. Fourier Transform–Infrared (FTIR) Analysis

Fourier transform–infrared (FT-IR) spectra of purified and lyophilized blank and quercetin loaded nanocapsules were obtained using an FTIR spectrophotometer (Perkin- Elmer, Norwalk). The same were obtained for starch, casein, SDS, conjugate, quercetin, Quercetin loaded nanocapsules and blank nanocapsules. To prepare sample for FTIR, a mixture of lyophilized sample and potassium bromide (KBr) was ground into a fine powder, compressed the powders at 20 psi for 10 minutes into a disc and the spectra were scanned at a resolution of 1 cm^{-1} over a wave number range of 600 to 3600 cm^{-1} and the characteristic peaks of IR transmission spectra were recorded.

6.4. *In silico* studies of biomolecule binding with nanocarrier

6.4.1. Molecular modeling

The model of casein micelle as proposed by Dalglesih, 2011 suggests that b-casein forms the inner core of a casein micelle. Therefore, it was hypothesized that b-casein will form the inner core of the polymeric Nanocapsules too. B-Casein micelle structure was modeled using iTASSER web based server (Roy et al., 2010), which is a protein structure modeling approach based on the secondary- structure enhanced profile–profile threading alignment (PPA) and the iterative implementation of the Threading Assembly Refinement (iTASSER) program.

b-casein amino acid sequence: P02666|CASB_BOVIN Beta-casein [Contains: Casoparan] - Bos taurus (Bovine).

MKVLILACLVALALARELEELNVPGEIVESLSSEESITRINKKIEKFQSEEQQTEDELQD
KIHPFAQTQSLVYPFPGPIPNLQNIPLTQTPVVVPPFLQPEVMGVSKVKEAMAPKHKE
MPFPKYVPEPFTESQSLTLTDVENLHLPLPLLQSWMHQPHQLPPTVMFPPQSVLSLSQS
KVLVPVQKAVPYPQRDMPIQAFLLYQEPVLPVVRGPFPIIV

6.4.2. Molecular docking calculations

Molecular docking calculations were carried out to visualize the binding site of quercetin to b-casein. All the docking calculations were performed by using CLC drug discovery workbench 2.4 (CLC Bio-Qiagen, Aarhus, Denmark). Protein models were first energy minimized in GROMACS 4.5.5 using OPLS force field (Spoel et al., 2005). The macromolecule was kept rigid, while all the torsional bonds of ligands were set free to rotate. Binding pockets were analyzed using the inbuilt analysis tool in CLC with a cut-off pocket size of 20Å° . Docking studies were visualized in CLC, and were performed at Intel(R) Core(TM) i3 CPU (3.20 GHz) with Microsoft Windows 7.

The active site residues were set in the search space inside a restriction sphere of radius 13Å° . The docking algorithm was set at a maximum iteration of 500 and run with virtual ligand screening mode. Ligand torsions were set free and docking was performed with a limit of five retained poses per molecule. For each compound the lowest energy pose was then selected from

these five solutions.

6.4.3. Molecular dynamics simulation

Molecular docking results determine a general binding mode of ligand. Nevertheless, MD simulation on the ligand–protein complex for further investigation of the effects of ligand binding on the conformation of protein was used. A 10 ns MD simulation was performed using the GROMACS 4.5.5 software package. The CharmM force field (Brooks et al., 1983) was used, and the Tip3p water model was employed for the water molecules. Because the system is required to be neutral for calculations, charges were balanced with sufficient amount of sodium counter ions. A cubic box was chosen, with periodic boundary conditions. The force field parameters of ligand were obtained from SwissParam web server (Zoete et al., 2011). At first the system was energy minimized using the steepest descent method. After energy minimization process, position restraint procedure was performed in association with NVT and NPT ensembles. An NVT ensemble was adopted at constant temperature of 300 K with time duration of 100 ps. After stabilization of temperature an isothermal–isobaric ensemble (NPT) was performed. In this phase a constant pressure of 1.0 bar was employed with time duration of 100 ps. NPT ensemble was finished after pressure stabilization. The Particle-Mesh Ewald (PME) method was used to treat the long-range electrostatic interaction and the cut-off method was used to treat the van der Waals interactions, with the cut-off distance of 1.0 nm.

The visualization of snapshots and trajectories at different time frames during the course of dynamics simulation was projected using visual molecular dynamics (Humphrey et al., 1996) and PyMOL (DeLano 2002) packages to get a pictorial depiction of the interaction. The MD trajectory for the system studied was used to extract the MD snapshots at different time spans, and these are discussed in detail in subsequent sections. MD simulations were performed on Ubuntu14.0 Linux operating system in a Intel(R) Core(TM) i7 CPU 3.20 GHz at the Bioinformatics Facility at the Department of Molecular Biology and Biotechnology, Tezpur University, India.

7. Salient Research Achievements:

7.1 Summary of Progress

Quercetin was identified as the potent flavanoid from among 32 polyphenolic compounds screened against the metalloproteinase enzyme *ADAM17*, thought to be responsible for the ectodomain cleaving of TNF alpha. Quercetin bound with the active site residue *GLU406* with a docking score of -60.41. Quercetin also displayed *ADAM17* selectivity over *MMP-1* and *MMP7*. Molecular dynamic simulations indicated that the whole system was stable and equilibrated. Extraction and purification of aglycone derivative of quercetin was performed using microwave assisted acid hydrolysis followed by SPME-RP-HPLC from *Capsicum chinense* fruit. Box-Behnken design and RSM optimization conditions of 74.38% solvent concentration, 1.75% acidification and 5.09 minutes of irradiation resulted in peak output of 0.29mg/gm aglycone quercetin. Furthermore, our results also provide direct evidence of the anti-inflammatory effects of quercetin on LPS induced experimental inflammation in THP-1 (differentiated macrophage) cells, which are mediated by the inhibition of the proinflammatory cytokine TNF-alpha.

Quercetin was encapsulated within the hydrophobic core of novel Casein-SDS nanocapsules of average diameter 450nm. As much as 0.74 ± 0.04 unit weight of quercetin was loaded into one unit weight of the conjugates. Quercetin loaded nanocapsules exhibited sustained release, tolerance to gastric digestion and displayed pH responsive release behavior.

7.2 New Observations:

7.2.1 *In silico* identification of natural biomolecules as selective ADAM17 inhibitors.

7.2.1.1 Virtual screening and Molecular docking studies

CLC Drug Discovery Workbench is part of the CLC bio Enterprise Platform. The molecular docking software based on a differential evolution algorithm; the solution of the algorithm takes into account the sum of the intermolecular interaction energy between the ligand and the protein and the intramolecular interaction energy of the ligand. The docking energy scoring function is based on the modified piecewise linear potential (PLP) with new hydrogen bonding and electrostatic terms included. Full description of the algorithm and its reliability as compared to other common docking algorithm can be found in literature (Thomsen and Christensen, 2006).

From initial validation of docking program it was observed that the docking program was able to reproduce the orientation of the co-crystallized Ligand (Figure 3). Thus it confirmed the efficiency of the docking program.

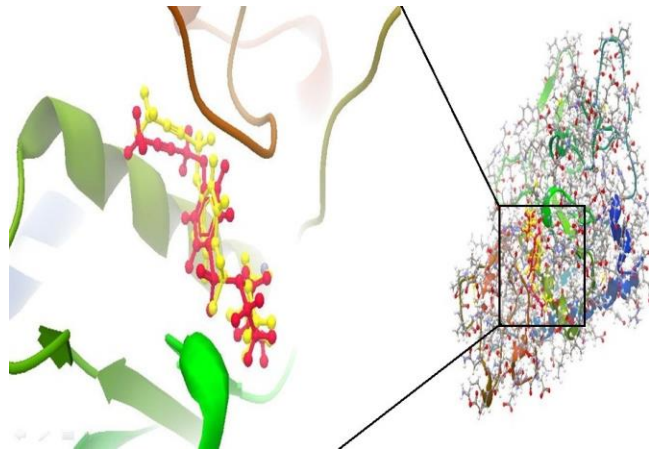


Figure 3. RMSD of complexed Aryl-sulphonamide complexed with 2OI0 after docking with CLC drug discovery workbench 2.4 at 500 iterations. Observed orientation of docked structure is very close to the orientation of the co-crystallized Ligand in the structure.

After lipinsky filtering, 25 compounds were carried forward for the docking calculations. 7 compounds in the total database of 32 compounds exhibited Lipinski violations. The Table 2 shows the list of compounds after Lipinski filtering.

Table 2: Compounds with no Lipinski violations.

PUBCHEM_CID	NAME	Atoms	Weight	Lipinski violations	Hydrogen donors	Hydrogen acceptors	LogP
1548994	Silymarin	57	482.441	0	5	10	1.88
969516	Curcumin	47	368.385	0	2	6	3.198
6914621	IK682	59	433.51	0	2	7	3.73
107971	Daidzin	50	416.382	0	5	9	1.694
9064	Catechin	35	290.271	0	5	6	1.414
5280445	Luteolin	31	286.239	0	4	6	3.927
445154	Resveratrol	29	228.247	0	3	3	3.123
5280443	Apigenin	30	270.24	0	3	5	4.282
5280343	Quercetin	32	302.238	0	5	7	3.572
5280863	Kaempferol	31	286.239	0	4	6	3.927
124052	Glabridin	44	324.376	0	2	4	3.886
5281607	Chrysin	29	254.241	0	2	4	4.637
5280961	Genistein	30	270.24	0	3	5	4.246
5281670	Morin	32	302.238	0	5	7	3.572
5281703	Wogonin	33	284.267	0	2	5	4.608
11349	3'-hydroxy-flavone	28	238.242	0	1	3	4.441
5280373	Biochanin-A	33	284.267	0	2	5	4.572
5281855	Ellagic acid	28	302.194	0	4	8	3.614
21676162	Quercetin 3'-sulfate	36	382.295	0	5	10	2.978
5281605	Baicalein	30	270.24	0	3	5	4.282
5472703	Paepalantine	36	302.282	0	2	6	3.967
637542	4-Coumaric acid	20	164.16	0	2	3	1.935
11092	Paeonol	22	166.176	0	1	3	1.771
54682930	4-hydroxycoumarin	18	162.144	0	1	3	2.817
323	Coumarin	17	146.145	0	0	2	3.172

Docking calculations were performed and the results are tabulated in table 3. Now only those molecules were carried forward who had binding interactions with the active site of 2OI0. The active site by the work of Moss et al., 1997 is Glutamic acid residue 406. In the table 6 are the molecules have active binding with the active site.

Table 3: Interaction of compounds with particular residues in the ADAMI7 catalytic cavity

PUBCHEM_C ID	NAME	2OI0 (ADAMI7)	Docking with GLU4 06	Interactions in the Catalytic site
---------------------	-------------	----------------------	-----------------------------	---

1548994	Silymarin	-72.15388	YES	TYR390, VAL343, MET345, GLU406, GLY349, ALA439
969516	Curcumin	-71.46606	YES	GLU398, LEU348, GLU349, GLU406, ASN447
6914621	IK682	-66.17677	YES	HIS405, LEU348, GLY349, GLU406
107971	daidzin	-65.85375	NO	VAL434, TYR436, ASN447, VAL440, ALA439, THR347
9064	Catechin	-63.55612	NO	LEU348, GLY349, HIS405, TYR436, VAL434, ASN447, VAL440
5280445	Luteolin	-63.55278	NO	gly349, leu348, GLY346, ASN447, ILE438
445154	Resveratrol	-62.02596	YES	TYR433, VAL440, GLY349, GLU406
5280443	Apigenin	-61.26228	NO	ASN447, GLY349, LEU348, GLY346
5280343	Quercetin	-60.41975	YES	GLY349, GLU406, HIS405, VAL434, ASN447, VAL440, TYR436
5280863	Kaempferol	-60.32962	YES	ASN447, VAL440, VAL434, HIS405, TYR436, GLU406, GLY349
124052	Glabridin	-60.24498	NO	THR347, HIS405, HIS415, ILE438
5281607	Chrysin	-59.82791	NO	GLY349, LEU348, GLY346,
5280961	Genistein	-58.74083	NO	ASN447, GLY349, LEU348, PRO437, ILE438, ALA439
5281670	Morin	-57.68926	YES	ALA439, LEU348, GLU406, GLY349, PRO437, GLY346,
5281703	Wogonin	-57.2775	NO	ALA439, GLY346, LEU348, GLY349,
11349	3'-hydroxy-flavone	-55.6906	YES	ALA439, LEU348, GLY349, GLU406,
5280373	Biochanin-A	-54.58596	NO	ALA439, PRO437, ILE438, GLY349, LEU438
5281855	Ellagic acid	-54.48186	NO	GLY442, ASN447, VAL440, ASN447, TYR436, VAL434, HIS405, GLU398
21676162	Quercetin 3'-sulfate	-53.34465	YES	GLU406, GLY349, GLY346, HIS405, TYR436, VAL434, ALA439, VAL440, ASN447
5281605	Baicalein	-52.38797	YES	GLU406, GLY349, LEU348,
5472703	Paepalantine	-51.66957	YES	ALA439, GLU406, GLY349, THR347
637542	4-Coumaric acid	-44.81328	YES	VAL434, LEU348, GLU406, GLY349
11092	Paeonol	-42.23919	YES	HIS405, GLU406, GLY349, LEU348
54682930	4-hydroxycoumarin	-40.94107	NO	GLY349, LEU348, ALA439
323	Coumarin	-39.5317	NO	NONE

Table 4: Docking scores of compounds with MMPs

PUBCHEM_CID	NAME	1HY7 MMP3	2Y6D MMP7	1I76 MMP8	2PJT MMP13	1RM8 MMP16	4H2E MMP9	1HFC MMP1	1QIB MMP2
1548994	Silymarin	-71.307	-67.1854	-69.4547	-67.9582	-72.3001	57.4334	61.0395	66.5665
969516	Curcumin	-73.285	-77.9395	-76.0567	-70.1417	-78.7159	59.2365	63.9117	-66.679
6914621	IK682	-78.3507	-70.4459	-69.9967	-72.4975	-68.5074	57.2953	67.2015	70.1614
107971	Daidzin	-78.6002	-73.5957	-79.1169	-72.5658	-75.9128	58.7177	61.1167	71.1942
9064	Catechin	-65.7462	-61.3177	-72.7691	-71.0079	-72.7413	58.9928	63.0995	63.5862
5280445	Luteolin	-73.827	-59.4029	-75.7915	-71.6798	-70.7754	60.2349	63.0674	66.7164

445154	Resveratrol	-67.4564	-58.2813	-69.5027	-69.7021	-68.8687	-	-	-	59.0871
5280443	Apigenin	-68.3323	-54.7364	-69.8069	-67.0466	-66.0311	-54.995	54.1018	-	62.6219
5280343	Quercetin	-69.8614	-57.5646	-73.3378	-71.6445	-67.84	58.4123	64.3829	-	65.4153
5280863	Kaempferol	-64.4171	-51.9968	-67.197	-65.7883	-63.618	-51.957	56.0798	-	61.3927
124052	Glabridin	-76.7161	-59.2596	-71.5736	-67.1459	-60.766	51.4356	61.0413	-	63.8268
5281607	Chrysin	-67.9759	-58.5565	-69.6716	-66.6017	-66.4087	54.8886	54.9869	-	62.9384
5280961	Genistein	-70.1483	-59.2643	-71.2546	-69.8248	-71.3991	55.0507	55.3028	-	67.4351
5281670	Morin	-65.8279	-54.3872	-70.9148	-67.7557	-68.7056	52.6551	58.1267	-	65.3686
5281703	Wogonin	-68.1321	-57.0665	-70.3525	-68.4415	-60.5438	-53.071	58.6656	-	63.9922
11349	3'-hydroxy-flavone	-63.285	-54.3843	-65.1321	-60.0819	-62.5321	47.8436	54.3915	-	60.7954
5280373	Biochanin-A	-73.0976	-61.9681	-72.2965	-70.2061	-71.1161	58.2952	53.3978	-	68.0032
5281855	Ellagic acid	-39.1078	-49.3468	-38.4283	-41.1249	-49.2757	35.3627	44.9468	-	41.4452
21676162	Quercetin 3'-sulfate	-61.766	-60.2341	-69.9534	-61.5956	-56.2349	50.4867	58.9488	-	67.2772
5281605	Baicalein	-67.5941	-58.175	-60.6434	-65.9966	-66.7742	53.4023	55.1832	-	60.8261
5472703	Paepalantine	-47.988	-61.247	-52.3518	-56.5918	-50.2057	47.9031	51.6149	-	47.7437
637542	4-Coumaric acid	-51.9033	-45.506	-50.6527	-51.8545	-52.3259	-43.578	45.6803	-	-48.612
11092	Paeonol	-50.3148	-48.3346	-50.6123	-48.5419	-54.0977	-37.611	47.1013	-	49.0082
54682930	4-hydroxycoumarin	-49.2316	-44.8977	-50.1893	-48.0923	-50.8934	38.2015	45.747	-	48.2485
323	Coumarin	-47.7792	-43.711	-46.9812	-45.7215	-48.9874	34.3077	46.4221	-	45.1708

Table 5: List of compounds indicated with “YES” as positively docked to the active site of ADAM17 and the particular MMP

PUBCHEM_CID	NAME	2O10 ADAM 17	1 HY7 MMP 3	2Y6D MMP 7	1I76 MMP 8	2PJT MMP1 3	1RM8 MMP1 6	4H2E MMP9	1HFC MMP1	1QIB MMP2
1548994	Silymarin	YES							YES	YES

969516	Curcumin	YES								
6914621	IK682	YES		YES	YES					
445154	Resveratrol	YES		YES						YES
5280343	Quercetin	YES	YES		YES	YES	YES	YES		YES
5280863	Kaempferol	YES	YES		YES	YES	YES	YES	YES	YES
5281670	Morin	YES								
11349	3'-hydroxy-flavone	YES	YES		YES	YES	YES	YES		YES
21676162	Quercetin 3'-sulfate	YES	YES			YES	YES	YES		YES
5281605	Baicalein	YES					YES			
5472703	Paepalantine	YES				YES	YES	YES	YES	YES
637542	4-Coumaric acid	YES	YES		YES	YES	YES			
11092	Paeonol	YES								

Table 6: Compounds showing + or – Blood brain barrier properties.

PUBCHEM_CID	NAME	Blood Brain Barrier
1548994	Silymarin	-
969516	Curcumin	+
6914621	IK682	-
445154	Resveratrol	+
5280343	Quercetin	-
5280863	Kaempferol	+
5281670	Morin	+
11349	3'-hydroxy-flavone	+
21676162	Quercetin 3'-sulfate	+
5281605	Baicalein	-
5472703	Paepalantine	-
637542	4-Coumaric acid	+
11092	Paeonol	+

Table 7: Pharmacokinetic properties of compounds as predicted by ADMETsar server.

ADMET	Quercetin	IK682	Baicalein	Paepalantine	Silymarin
Blood Brain Barrier	-	-	-	-	-
Human Intestinal Absorption	+	+	+	+	+
Aqueous Solubility LogS	-2.9994	-3.6098	-2.9994	-3.294	-2.6488
AMES Toxicity	-	-	-	-	-
Carcinogenic	-	-	-	-	-

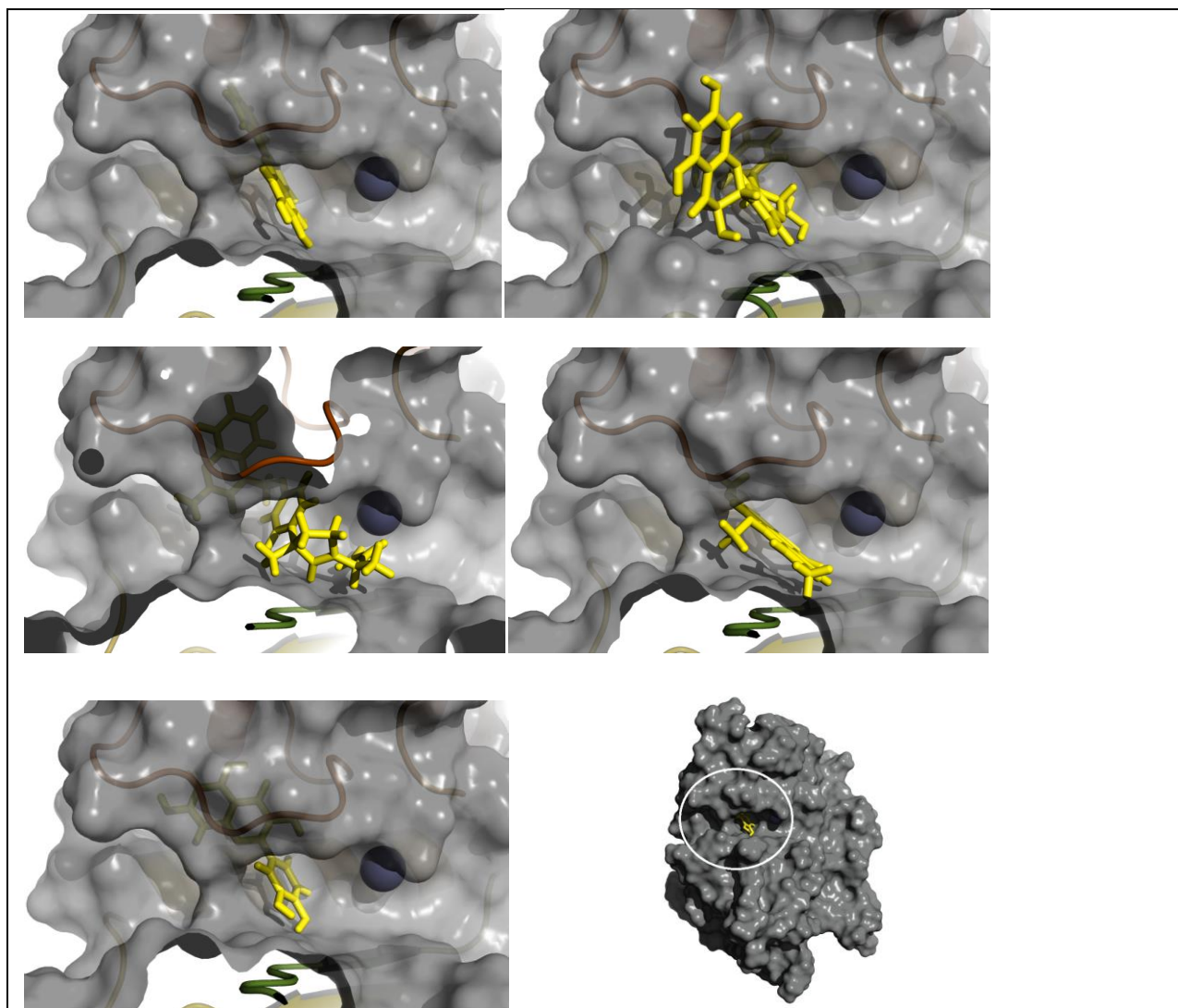


Figure 4: Docking poses of the top: Baicalein, Silymarin, IK682, Paepalantine, Quercetin and Quercetin docked (view zoomed out).

In the present study, we report selective ADAM17 inhibitors obtained through high throughput screening of polyphenolic database. The database was screened for ADAM17 inhibitory activity by applying various filters like HTS docking for ADAM17 and MMPs and violation of Lipinski's rule of five to obtain the selective ADAM17 inhibitors over various MMPs (MMP1, 2, 3, 7, 8, 9, 13, and 16). One partly selective ADAM17 inhibitors is reported having good pharmacokinetic properties as well as good interaction with the active site of ADAM17. Compounds Quercetin could serve as excellent lead molecules for the development and can be further improved for selective ADAM17 inhibitors. Docking studies were carried out with known ADAM17 inhibitors to validate the docking protocol which was used as one of the constraint parameter for carrying out the virtual screening. The docking scores obtained for these compounds are in consonance with that of the experimental values, thus validating the docking protocol. Since selectivity is an important issue for ADAM17 inhibitors, efforts have been made

to report more selective ADAM17 inhibitors over MMPs. However, keeping in mind pharmacokinetic parameters in mind and effective docking to ADAM17 catalytic site, certain high selective compounds like curcumin have been set aside. Lipinsky filters, docking to active site of ADAM17, docking to active sites of MMPs, Blood brain barrier permeability and pharmacokinetic parameters have been used as filters as shown in table (4, 5, 6, 7, 8, 9). Among the top 5 best ligands selected, quercetin was visualized to dock more effectively in the active site cavity of ADAM17. Quercetin formed H-bond with Val 440, Asn 447, Tyr 346, Val 343, His 405, Gly 349 and Glu 406.

Orientations of the active and inactive compounds in the active site of ADAM17 supported the information to prove the activity profile of the said compounds.

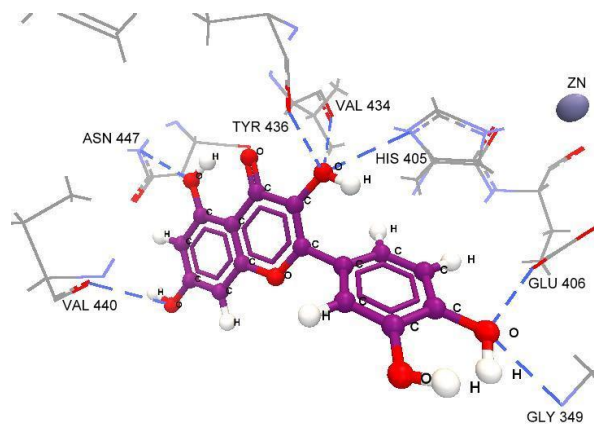


Figure 5: Showing interaction of quercetin with amino acid residues in the catalytic cavity of ADAM17.

7.2.1.2 Molecular Dynamic simulations and trajectory analysis

The trajectories were stable during the whole production part of the 10,000-ps MD simulation run. The trajectory stability was checked and corroborated by the analysis of the root mean square deviation (RMSD) (Fig. 6) as functions of time for ADAM17 and its complexes with quercetin. The analysis of Fig. 14 indicates that the RMSD of all systems reached equilibrium and oscillated around the average value. This evidence clearly indicates that the whole system was stable and equilibrated.

In the present MD study, the radius of gyration (R_g) values of quercetin and ADAM17–quercetin complexes were determined and plotted as a function of time, as shown in Fig. 7.

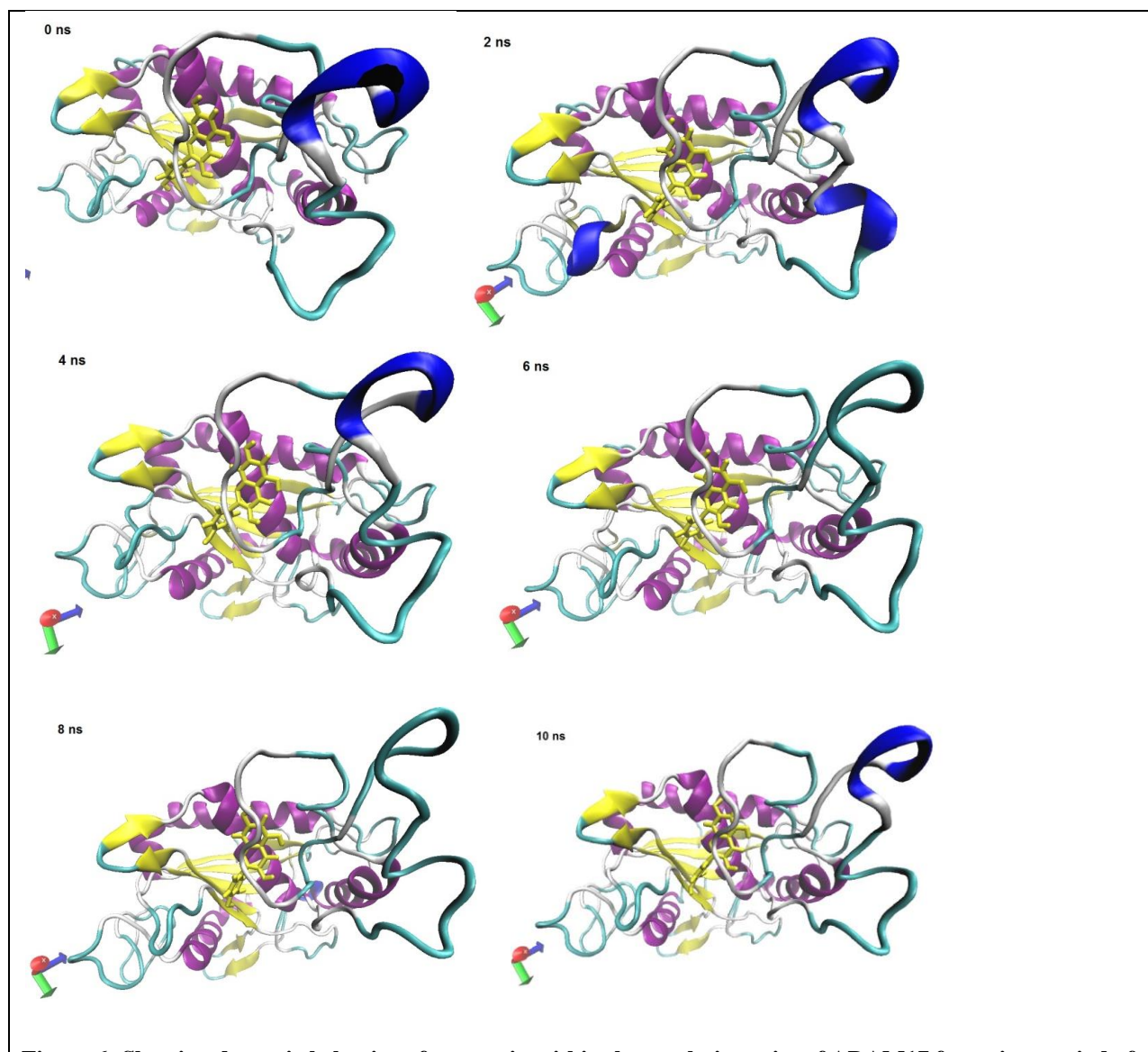


Figure 6: Showing dynamic behavior of quercetin within the catalytic cavity of ADAM17 for a time period of 10 ns.

In the systems, the R_g values were stable, indicating that the MD simulation achieved equilibrium.

Local protein mobility was analyzed by calculating the time-averaged root mean square fluctuation (RMSF) values of ADAM17–quercetin complexes. The results were plotted against residue numbers based on 10,000-ps trajectory (Fig. 7). . The obtained results clearly indicate that the residues at the binding site had low fluctuations for the ligand. Also, the structure of ligand binding site remained approximately rigid during simulation.

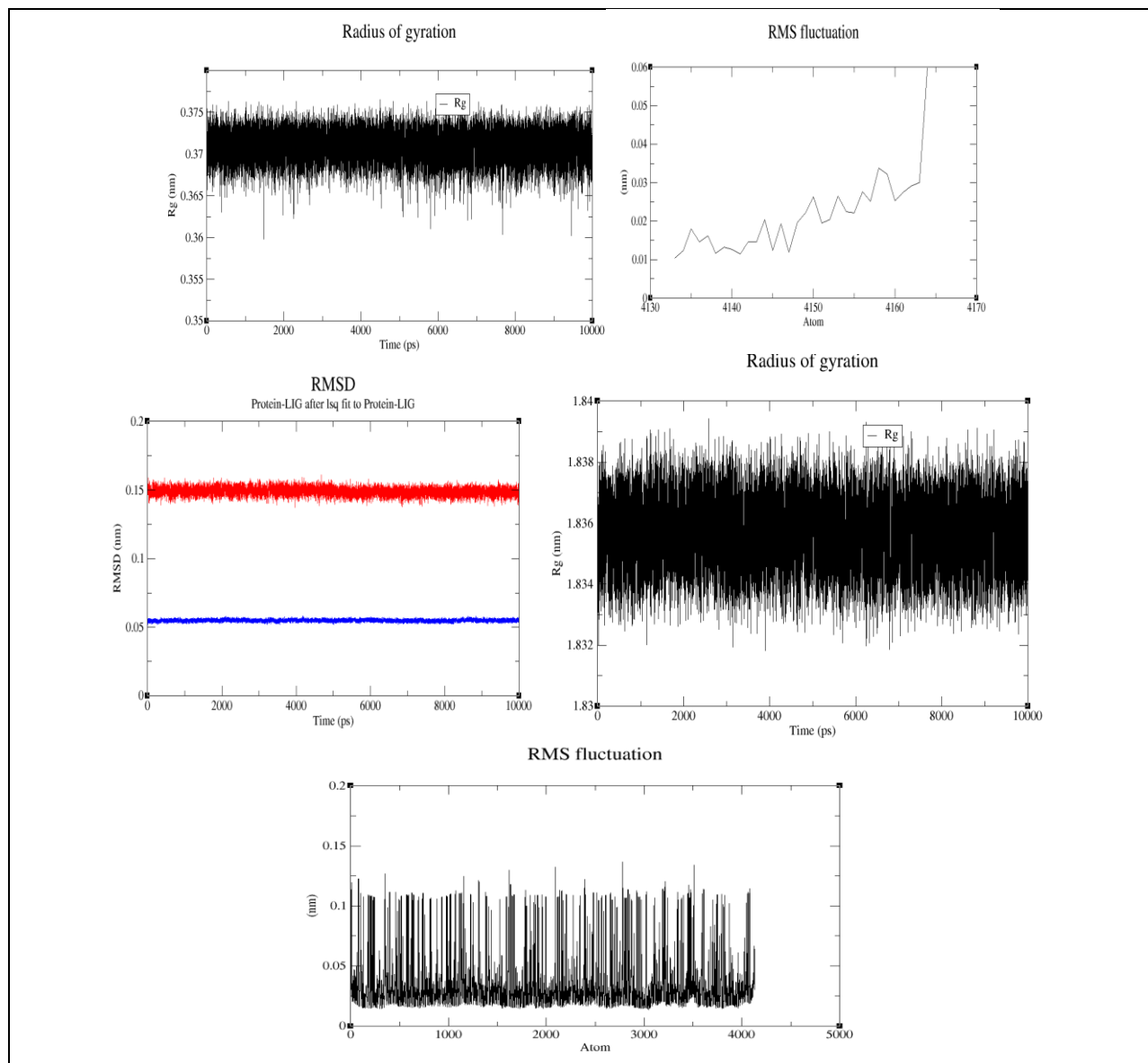


Figure 7: GROMACS dynamic analysis of from top; Quercetin gyration, Quercetin RMSF, ADAM17 (Red)-Quercetin (Blue) RMSD, ADAM17 gyration, ADAM17 RMSF.

7.2.2 Screening, Extraction and Purification of natural biomolecule from locally available medicinal plants

7.2.2.1 Screening of medicinal plants of Assam

P. microcephalum is believed to be appetizer and it reliefs from acidity in stomach. Leaves of *M. oleifera* leaf are believed to cure jaundice and prevent viral infection that causes measles. Capsicum chinense is also believed to have medicinal properties and is considered beneficial for

the stomach. Total flavanoids were estimated in the three, and were found to be *P.microcephalum* 36.6 ± 2.45 mg quercetin equivalent/gm, *C. chinense* 52.12 ± 3.56 mg quercetin equivalent/gm and *M. oleifera* 39.0 ± 3.21 mg quercetin equivalent/gm. The results of *P.microcephalum* and *M. oleifera* are in correlation to the findings of Saikia et al., 2011.

Total flavanoid content of *C. chinense* was found to be the highest, and therefore it was considered for further optimization, extraction and purification studies.

7.2.2.2. Effect of acid hydrolysis on Quercetin content

HPLC analysis confirmed the acid hydrolysis of quercetin glucosides to aglycone quercetin, as there was clear increase in aglycone quercetin fractions and decreases in certain other peaks which were not characterized due to lack of standards. As shown in figure 8, the glucose moieties were cleaved off by the process of microwave assisted acid hydrolysis, and thereby increasing the yield of aglycone quercetin.

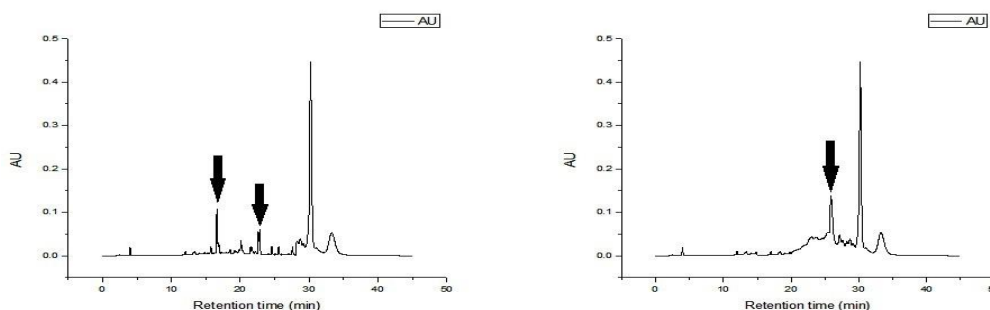


Figure 8: HPLC chromatogram showing acid hydrolysis of quercetin glucosides into aglycone quercetin.

This could be attributed to the protonation of the solvent by the added acid. The protons would attack the lone pair oxygen in the C-O-C bond, and thereby destabilize it. This destabilization usually leads to bond breakage and release of the glucose fraction from the quercetin glucoside.

7.2.2.3. Diagnostic Checking of Fitted Models and Response Surfaces

The experiment design and the respective response data for the extraction of aglycone quercetin compounds from *C. chinense* are shown in table 2. The coefficient of regression of the intercept, linear, quadratic and interaction terms of the model were calculated using the least square technique and are shown in table 8.

Table 8. Experimental design in uncoded forms and effect of process variables of maah on responses.

Uncoded Process Variables	Response
---------------------------	----------

Concentration	Time	Acidification	Quercetin (Actual)	Quercetin (Predicted)
%	Minutes	%	mg/g	mg/g
50	2	1.5	0.25	0.22
100	2	1.5	0.18	0.1575
50	8	1.5	0.14	0.1625
100	8	1.5	0.18	0.21
50	5	1	0.18	0.17375
100	5	1	0.18	0.16625
50	5	2	0.23	0.24375
100	5	2	0.23	0.23625
75	2	1	0.15	0.18625
75	8	1	0.18	0.16375
75	2	2	0.22	0.23625
75	8	2	0.29	0.25375
75	5	1.5	0.26	0.298
75	5	1.5	0.3	0.298
75	5	1.5	0.29	0.298
75	5	1.5	0.31	0.298
75	5	1.5	0.33	0.298

Table 9: Estimated regression coefficients for the quadratic polynomial model and the analysis of variance (anova) for the experimental results.

Source	Sum of Squares	DF	Mean Square	F Value	Prob > F
Model	0.047789	9	0.005309902	4.08229695	0.0385
A	0.000113	1	0.0001125	0.086490939	0.7772
B	1.25E-05	1	1.25E-05	0.009610104	0.9247
C	0.0098	1	0.0098	7.534321801	0.0287
A2	0.014042	1	0.014042368	10.79589005	0.0134
B2	0.011716	1	0.011716053	9.007399058	0.0199
C2	0.005232	1	0.005231842	4.022283881	0.0849
AB	0.003025	1	0.003025	2.32564525	0.1711
AC	0	1	0	0	1.0000
BC	0.0004	1	0.0004	0.307523339	0.5965
Residual	0.009105	7	0.001300714		
Lack of Fit	0.006425	3	0.002141667	3.196517413	0.1455
Pure Error	0.00268	4	0.00067		
Cor Total	0.056894	16			
			R-Squared	0.839965881	

		Adj R-Squared	0.634207728	
C.V. 15.72082		Adeq Precision	5.079369769	

* Significant at the 99% level if P value < 0.01 and 95% level if P value < 0.05 .

SS sum of squares; DF Degree of Freedom

The correlation coefficients for the responses quercetin extraction ($R^2 = 83\%$) are quite high for response surfaces and indicate that fitted quadratic model accounted for more than 90% of the variance in the experimental data, which were found to be highly significant.

F -value for the lack of fit was insignificant ($P > 0.05$) thereby confirming the validity of the model. The model F value of 4.08 implies that the model is significant. The value of coefficient of variation (C.V.) was 15.72%, suggested that the model was reliable and reproducible. The results indicated that the model could work well for the prediction of quercetin extraction from *C. chinense*.

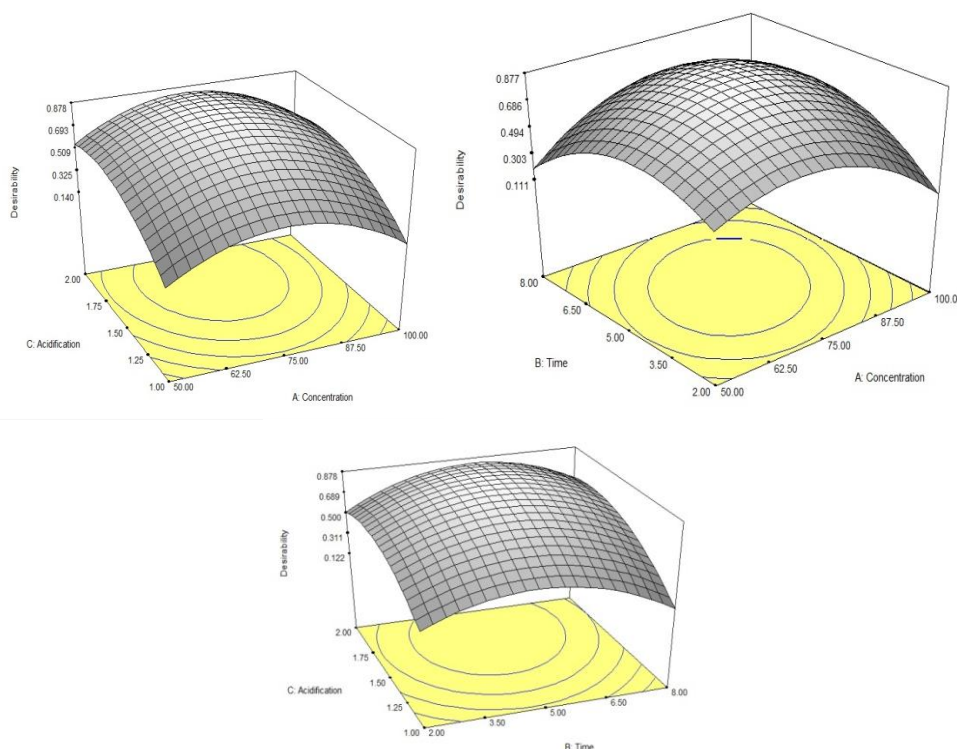


Figure 9: Analysis of Response surfaces and the influence of solvent concentration (%), solvent to sample ratio (v/w) and radiation time (min) on quercetin extraction

In order to investigate the interactive effects of operational parameters on quercetin extraction, the three-dimensional response surface plots were generated by plotting the response (percentage conversion) on the Z-axis against two independent variables while keeping the other independent variable at its zero level. Fig. 9 depicts the interactions between solvent conc. and each of the other factors (acidification and irradiation time) on the quercetin extraction profile.

7.2.2.4. Optimization of extraction process: Verification of predictive model

The optimization of the process variables, i.e., solvent concentration, acidification and irradiation time, was done using a superimposed graph to find out the conditions when we can get the best results for quercetin extraction. Optimization was done for obtaining maximum quercetin in minimum time. The optimal conditions of quercetin extraction for quercetin extract obtained using response surface methodology were as follows: solvent concentration= 74.38%, irradiation time= 5.09 minutes and acidification was 1.75%. The suitability of the model equation for predicting the optimum response values was tested using the selected optimal conditions. The predicted extraction yield of quercetin was 0.31 mg/gm, which was consistent with the practical extraction yield of quercetin of 0.29 mg/gm. The strong correlation between the real and predicted results confirmed that the response model was adequate to reflect the expected optimization.

7.2.2.5. Physical and Chemical Characterization of isolated compounds

Extraction was carried out using the optimized protocol, and fractionated using SPME. The SPME fraction was concentrated 10 folds, and then injected into the RP-HPLC system running at same conditions. Pure fractions were repeatedly collected as they came out the detector. The pool of mobile phase collected containing the biomolecule was freeze dried and biomolecule was recovered as yellow, crystalline powder. Although current purification techniques make use of preparative HPLC systems, because of our instrumental limitation, we had to restrict our collection techniques in this way. However, the technique does not compromise to the consistency of the reported results.

The HPLC chromatograms show a distinct peak in the purified fraction at the same retention time as that of quercetin.

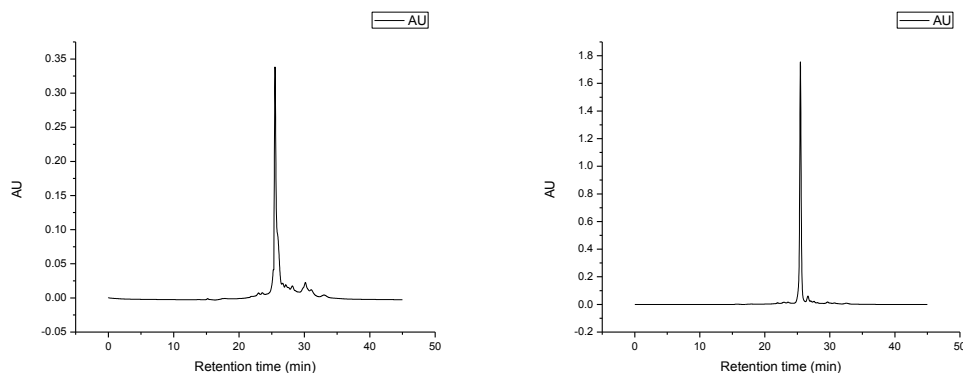


Figure 10. HPLC chromatogram showing (a) Purified quercetin, (b) standard quercetin.

The isolated constituents of quercetin were identified through IR spectroscopy by comparing with IR charts to assign their identities. FTIR of isolated quercetin is shown in Figure: 11. The broad band around $3420\text{--}3440\text{ cm}^{-1}$ that is characteristic for hydroxyl group indicates the presence of phenolic compounds. The observed absorption band at 1628 cm^{-1} indicates N-H bend, shows the presence of primary amines. Strong band in the region (1608 cm^{-1}) confirms the presence of C---O Aromatic ring stretch. Absorption at 1383 cm^{-1} is the most characteristics of O-H bending of phenols. Strong band at 1318 cm^{-1} indicates C-H bond in aromatic hydrocarbon. Appearance of strong band at 1265 cm^{-1} is due to C=O stretching of aryl ether. Absorption around 1203 cm^{-1} could be due to C=O stretch caused by phenols. Absorption around $1167, 940$ and 677 cm^{-1} may be due to C-CO-C stretch and bending in ketones and C-H bending of aromatic hydrocarbons.

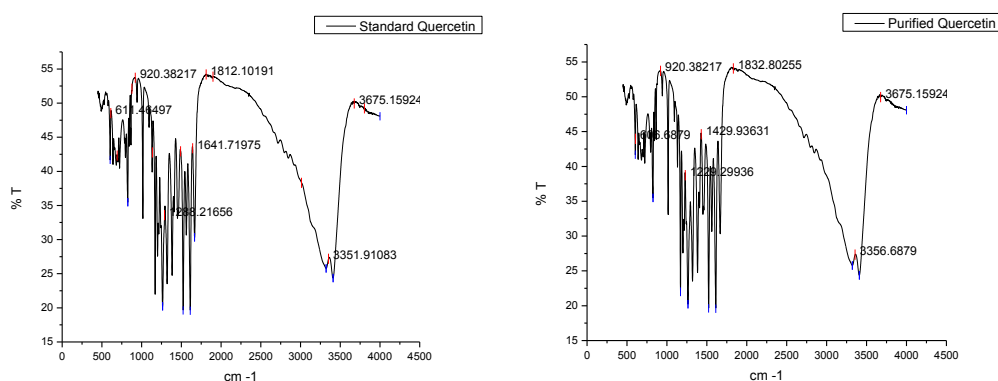


Figure 11: FTIR spectra of purified quercetin and standard quercetin.

The structural identification of each compound was carried out by ^1H NMR and ^{13}C NMR. Purified compound was isolated as a yellow amorphous powder. The ^1H -NMR spectrum (Figure 12) of the compound isolated from the extract revealed H-6 Φ -H-6 Φ ortho-coupling (8.4 Hz) at 7.4 and 6.8 p.p.m., and H-6 Φ -H-2 Φ metacoupling (2 Hz) at 7.4 and 7.6 p.p.m. Another metacoupling occurs between H-6 and H-8 (1.9 Hz) at 6.3 and 6.5 p.p.m.

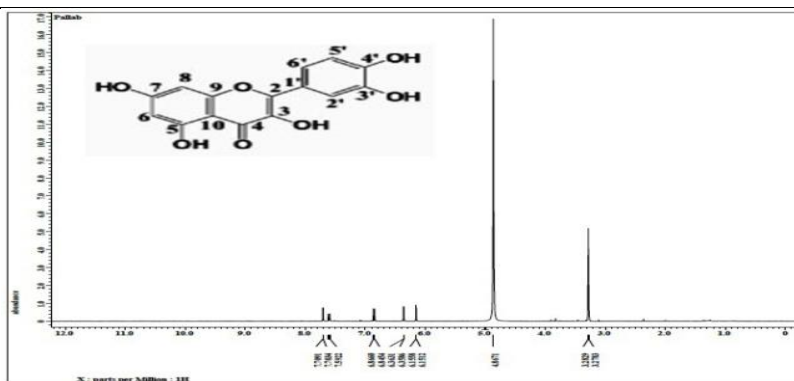


Figure 12: ^1H NMR spectra of purified Quercetin extract.

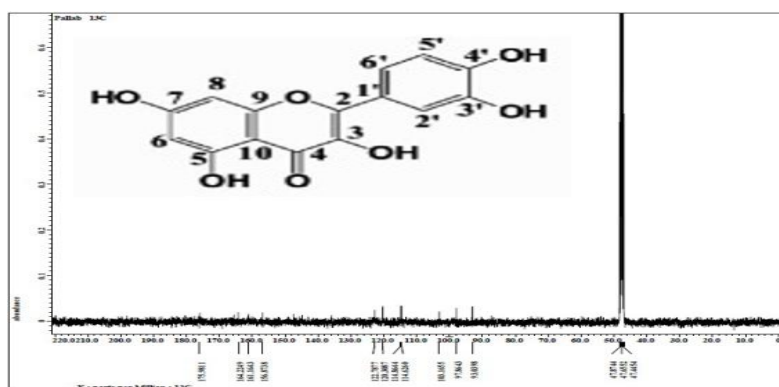


Figure 12a: ^{13}C NMR spectra of purified Quercetin extract.

The ^1H -NMR and ^{13}C -NMR spectrums (Figure 12 and 12a) of purified quercetin exhibited resonances due to aromatic systems. In the ^1H -NMR spectrum of 1, the aromatic region exhibited an ABX system at 7.73 (^1H ,d,J=2.0Hz,H-20), 7.62 (^1H ,dd,J= 2.0 and 7.5 Hz, H-60), and 6.87 (^1H ,d,J=8.0Hz,H-50) due to a 30,40 di-substitution of ring B and a typical meta-coupled pattern for H-6 and H-8 protons (6.17 and 6.37,d,J= 2.0 Hz). The ^{13}C NMR spectrum of compound showed the presence of 15 aromatic carbon signals. Based on the NMR data and comparison of the data given in the literature, the structure of purified compound was identified as quercetin. These results are identical in every respect with those obtained for the reference sample of quercetin.

7.2.2.6. Modulating effects of quercetin on the expression of TNF alpha in LPS stimulated THP-1 macrophages

Data presented in Fig. 13 show the effects of quercetin (8 h) on TNF-alpha protein expression by THP-1 differentiated macrophage cells as detected by ELISA analysis. Figure 7 shows inflammation related TNF alpha expression of $1 \mu\text{g ml}^{-1}$ LPS-stimulated THP-1 macrophages

with (a) Control: No LPS-No Quercetin, (b) Q: 100 μM Quercetin (c) LPS: LPS treatment (d) Q+LPS: co-incubation of 100 μM Quercetin-LPS. Data demonstrate (Fig. 7) that quercetin at 100 μM downregulated TNF-alpha protein expression by THP-1 differentiated macrophage cells. The TNF-alpha expressed in quercetin treated inflammation was lower than basal TNF-alpha levels in non-LPS treated cells.

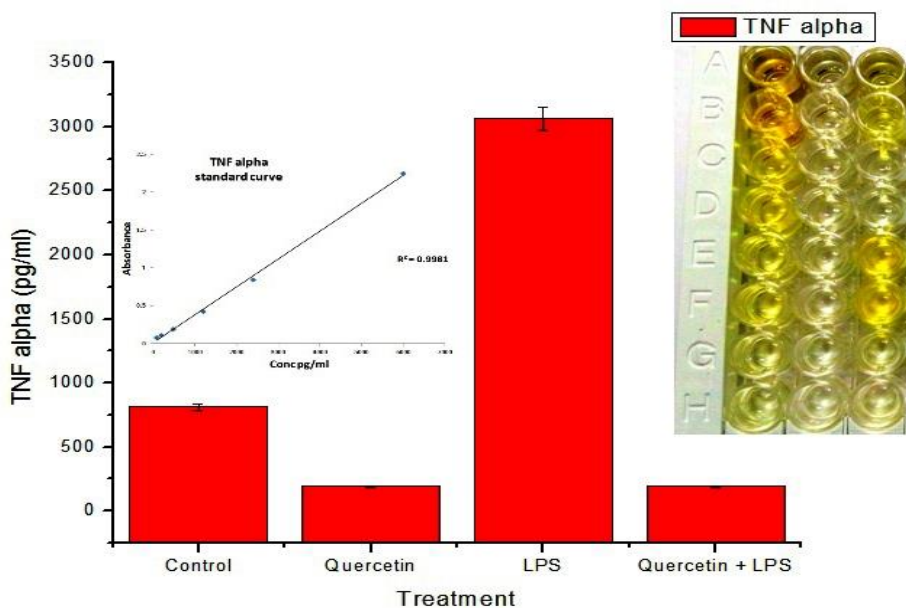


Figure 13: Inflammation-related TNF alpha expression of 1 $\mu\text{g ml}^{-1}$ LPS-stimulated THP-1 macrophages with (a) Control: No LPS-No Quercetin, (b) Q: 100 μM Quercetin (c) LPS: LPS treatment (d) Q+LPS: co-incubation of 100 μM Quercetin-LPS. Data shown are the means + standard deviation (SD bars) from independent biological replications. TNF alpha standard linear regression $R^2 = 0.998$.

Our findings suggest that the cytokine TNF-alpha can be inhibited by quercetin. Although the results of this study are preliminary, we believe that quercetin-induced suppression of TNF-alpha can result in the stimulation of anti-inflammatory cytokines via inhibiting the activation of NF-kB, and therefore, we anticipate that quercetin can be widely used as an anti- TNF-alpha therapy. Evaluation of the molecular mechanisms of quercetin-induced anti-inflammatory effects may be a promising area for the development of new flavonoid-based biopharmaceutical Biofunctional foods for the treatment of various inflammatory diseases including inflammatory bowel diseases.

7.2.3. Development of colon targeted nanocarrier as biomolecule delivery vehicle.

7.2.3.1. Isolation of casein from cow milk and its characterization

The SDS results confirmed the purity of the extracted casein molecule and two distinct bands were observed near the 25 and 30 kDa regions of the standard ladder. The figure 22 shows the

SDS PAGE results of the isolated casein protein.

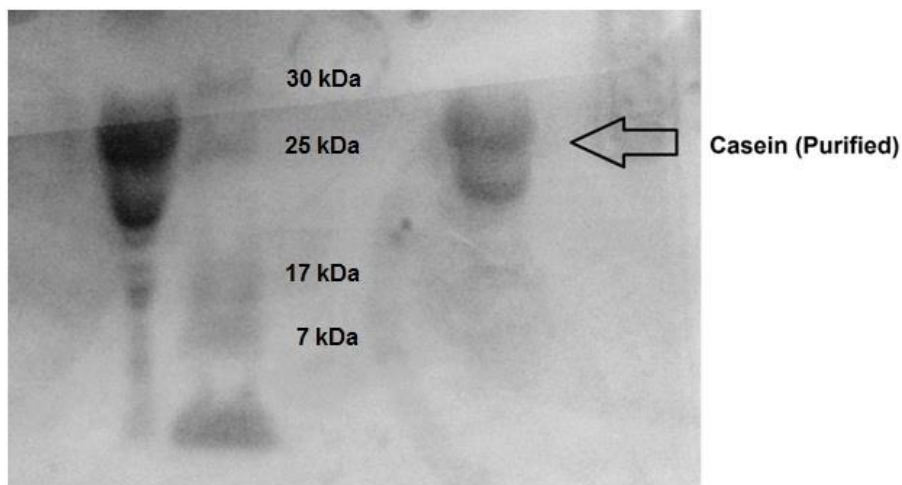


Figure 14: SDS–PAGE analysis of purified Casein (lane 1, casein concentration of $10\text{mg}/\text{mL}^{-1}$), purified casein (1/10 dilution) (lane 3) and pre-stained protein marker low range (Lane 2). In each lane, $10\mu\text{L}$ of the sample.

7.2.3.2. Isolation of starch

Native starch was isolated from waxy rice variety of Assam, India (Bora Saul) and successive treated to produce slow digestible starch.

7.2.3.2.1. Effect of the temperature-cycled treatments on the yield of SDS

The present data showed that there was a maximum yield of SDS for the product with the temperature cycle of $4/45\text{ }^{\circ}\text{C}$ (Fig. 15). Initial retrogradation at a lower temperature ($4\text{ }^{\circ}\text{C}$) favored the nucleation of amylopectin crystallites, while it could reduce the propagation rate of the crystallites based on the former nucleation. A higher temperature, therefore, is needed to promote the propagation process. There was, finally, an equilibrium occurring between the nucleation and the propagation rates during the temperature-cycled treatment. A suitable temperature cycle at the equilibrium state could accelerate the formation of the imperfect crystallite that was one of the main components for the SDS.

The yield of SDS in % was seen to be highest at the temperature cycle of $4/45^{\circ}\text{C}$. The SDS yield was similar in the $4/35^{\circ}\text{C}$ range. However there was a sharp decline in SDS yield beyond $4/45^{\circ}\text{C}$. SDS yield was also dramatically very less at $4/25^{\circ}\text{C}$.

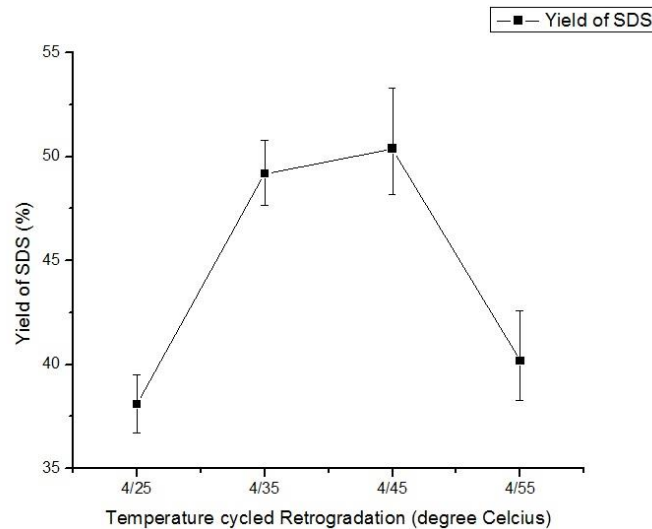


Figure 15: Effect of different temperature cycles on the yield of the SDS products obtained using a starch to water ratio of 1:3 (w/v); with a time interval of 24 h for 7 d (data shown were expressed as means \pm standard deviations of at least triplicate).

7.2.3.2.2. Effect of the temperature-cycled time on the yield of SDS

The results demonstrated that the maximum SDS yield of 82.7% was observed for the product subjected to the temperature-cycled time of 30 days (Fig. 16). It is generally recognized that the gelatinized amylose can be organized into a crystalline area completing in several hours, while amylopectin recrystallization needs several days or more than 1 month. Nevertheless, long-term retrogradation (i.e. 21 d) could promote the formation of the perfect crystallites of amylopectin and increase the yield of resistant starch (RS). These results suggest that an appropriate retrogradation time could induce the interaction between crystalline area and amorphous starch fractions and result in the higher yield of SDS.

On establishing the conditions for highest yield at 4/45°C, optimization was carried out for temperature cycled days. From the experimental results it was observed that SDS yield was highest at day 5. Beyond which there was decline till day 15. However the SDS yield was seen to increase further till day 25 and then finally subsided again till day 30.

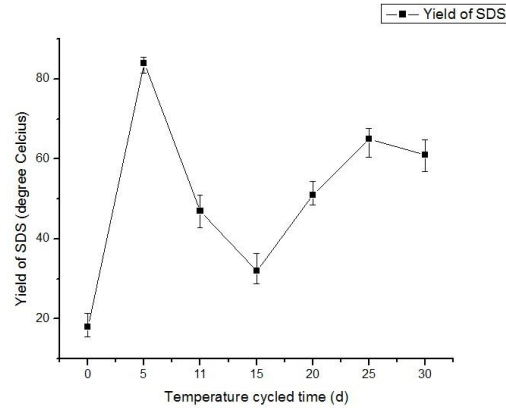


Figure 16: Effect of different temperature-cycled time on the yield of the SDS products obtained using a starch to water ration of 1:3 (w/v); at 4/45°C with a time interval of 24 h for 0, 5, 10, 15, 20, 25 and 30 d.

7.2.3.2.3. Effect of different water contents on the yield of the SDS

The results showed that water content at 1:3 (w/v) samples to solvent could produce a maximum SDS yield of 82.7% SDS (Fig. 17). Water molecules have twofold effects in a retrograded starch system: one is as a solvent to make starch molecules migration and another role is incorporated into starch recrystallization (Jin et al., 2011). The migration rate might be reduced, while the water content was lower (i.e. starch to water, 1:1). The higher water contents (i.e. starch to water, 1:3, 1:4, and 1:5) made a dilute effect to reduce the retrogradation of starch and the retrogradation of amylopectin was not observed for more than 80% water (Zhou et al., 2011), although they could increase the migration rate of starch molecules.

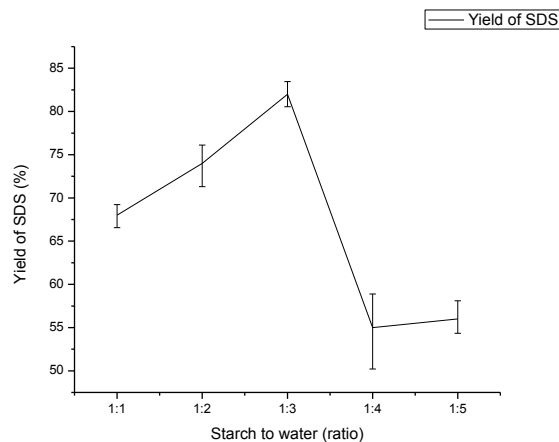


Figure 17: Effect of different water contents on the yield of the SDS products obtained using a starch to water ratio of 1:1, 1:2, 1:3, 1:4, and 1:5; at 4/45 °C with a time interval of 24 h for 5d.

7.2.3.2.4. Structural characterization of the SDS product

From the FTIR analysis the peak at 700 cm⁻¹ is clear indicative of carbohydrates and starches. Shifts in peak were observed at 1800-2200 cm⁻¹ range which might be attributed to change in the branch chains of amylopectin starch, or due to possible bond formation between the chains, during the development and propagation of nucleation of starch.

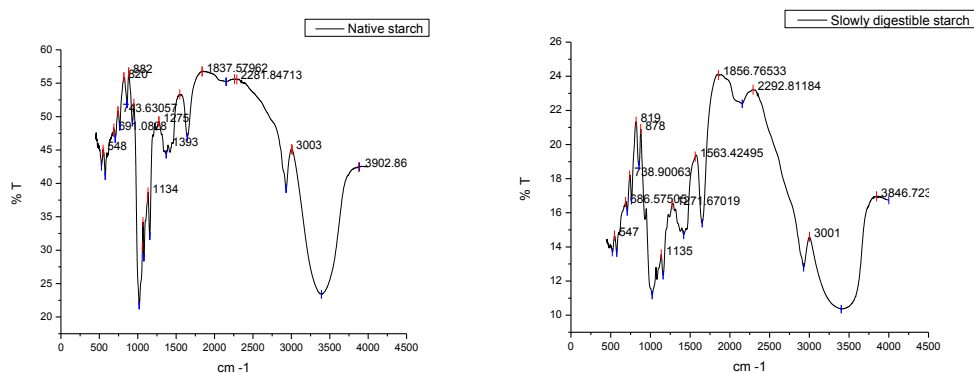


Figure 18: FTIR spectra of native and SDS product.

7.2.3.2.5. Characterization via scanning electron microscopy and imaging

The SEM images revealed that the SDS product with the temperature-cycled retrogradation after hydrolysis for 20 min had a more smoothing surface than that with the isothermal treatment (Fig. 19). The smoothing surface could reduce the chance of starch to contact with the enzymes. There were only several laminated structures of the non-digestible starch remaining in the SDS product with the isothermal retrogradation after the hydrolysis for 60 min and 120 min. Nevertheless, a number of solid connection parts were observed for the SDS product with the temperature-cycled treatment after the hydrolysis for 60 min (Fig. 19). These solid parts still existed and transformed to solid blocks with a smaller size, while the SDS product was hydrolyzed for 120 min (Fig. 19). These results suggest that the temperature-cycled treatment could yield the imperfect crystallites and provide the protection for the amorphous starch against the enzymes.

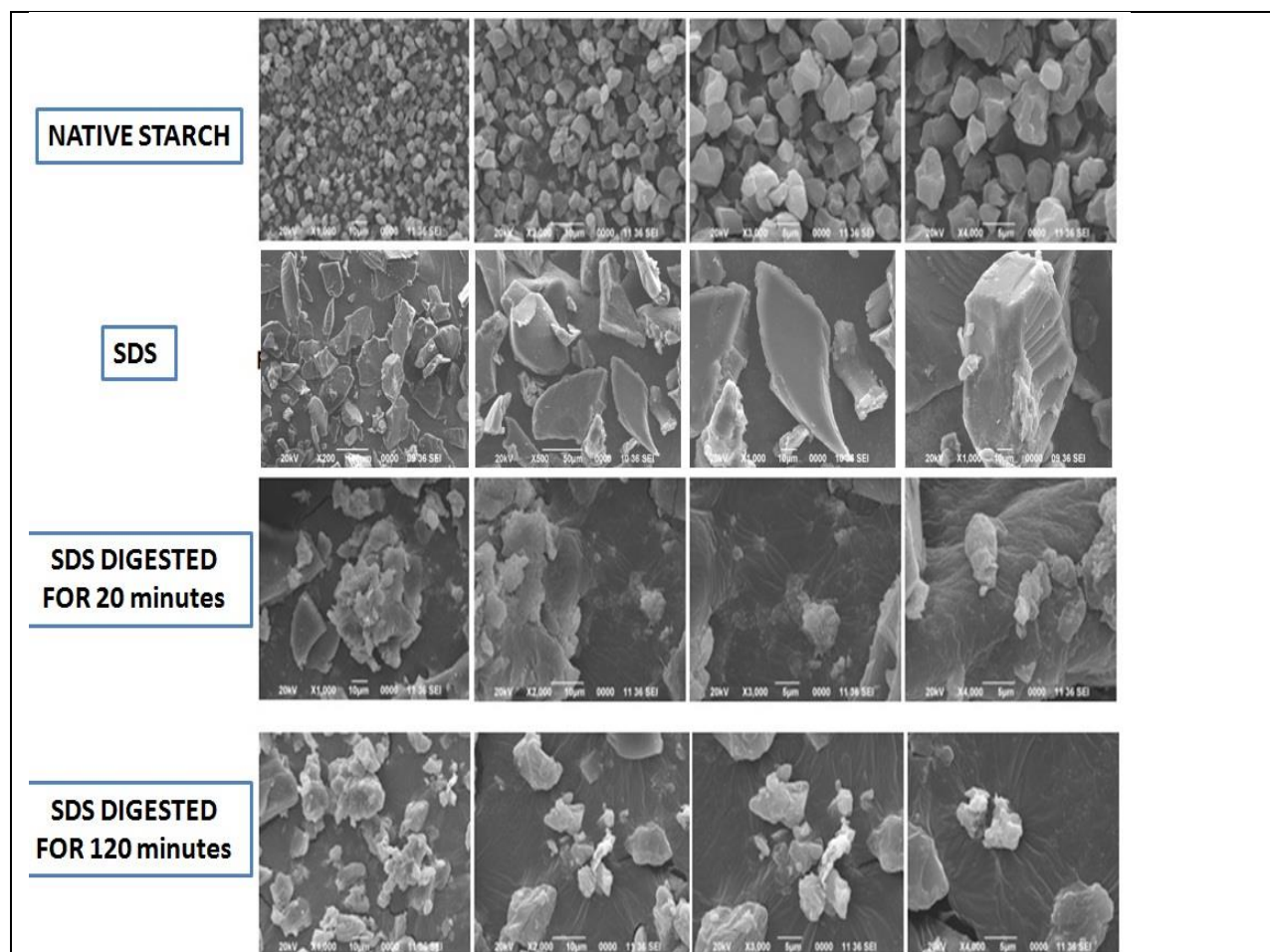


Figure 19: SEM images showing (Row 1) the native starch isolated from *Oryza glutinosa* Lour. Poaceae waxy rice, (Row 2) the SDS products using a starch to water ratio 1:3 (w/v) with temperature-cycled (4/45 °C), (Row 3) the SDS product using a starch to water ratio 1:3 (w/v) with temperature-cycled (4/45 °C) retrogradation after hydrolysis for 20 min, (Row 4) the SDS product using a starch to water ratio 1:3 (w/v) with temperature-cycled (4/45 °C) retrogradation after hydrolysis for 120 min.

7.2.3.2.6. Molecular Weight characterization of Starch and the SDS product

The HPGPC analysis revealed shift in molecular weight of native and SDS product. The native starch had molecular weight in around 9109 Da. Whereas, in the SDS product there was an increase in molecular weight. The molecular weight of SDS product was characterized at 104273 Da. This was a tremendous increase in molecular weight. It can be hypothesized that the bonding of amylopectin chains produced this enormous shift in molecular weight change.

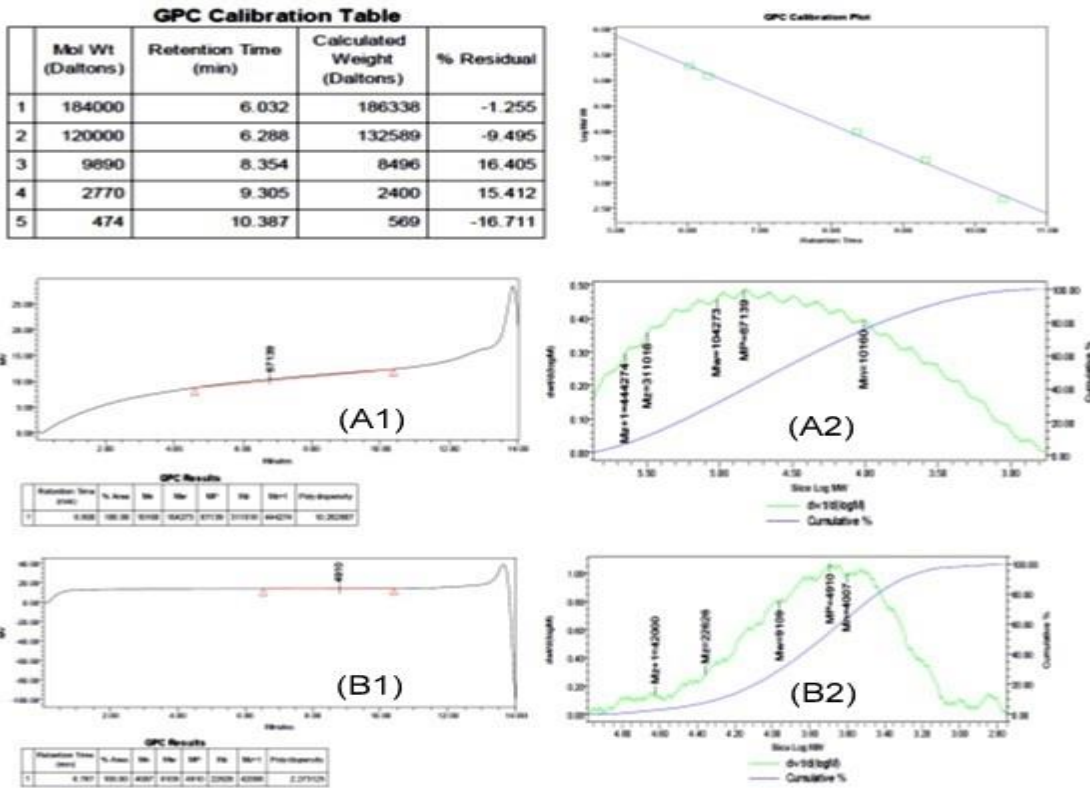


Figure 20: GPC spectrum showing (A1 and A2) the SDS product using a starch to water ratio 1:2 (w/v) with temperature-cycled (4/45 °C) retrogradation, and (B1) and (B2) the native starch isolated from *Oryza sativa* var *glutinosa* waxy rice.

7.2.3.3. Preparation of Casein-graft SDS Copolymer with the Maillard Reaction.

The Maillard reaction was used to graft SDS to casein. For our solid phase Maillard reaction of casein with SDS at 60°C and a relative humidity of 78.9%, we found that the reaction rate was moderate and the side reactions were not obvious at neutral pH. Therefore, pH 7.0 was chosen in the Maillard reaction studied below. After the Maillard reaction, SDS–PAGE analysis was performed to monitor the molecular weight of the resultant species. Figure 1 shows that two bands from the four casein constituents as indicated in the literature (Shephard 2000) appear before the reaction. After the reaction, a smear that exhibits larger molecular weight than casein appears. As the reaction time increases, this smear becomes clearer and wider while the two casein bands become faint. This indicates that, the longer reaction time is, the more SDS molecules conjugate to casein and a larger molecular weight copolymer is produced.

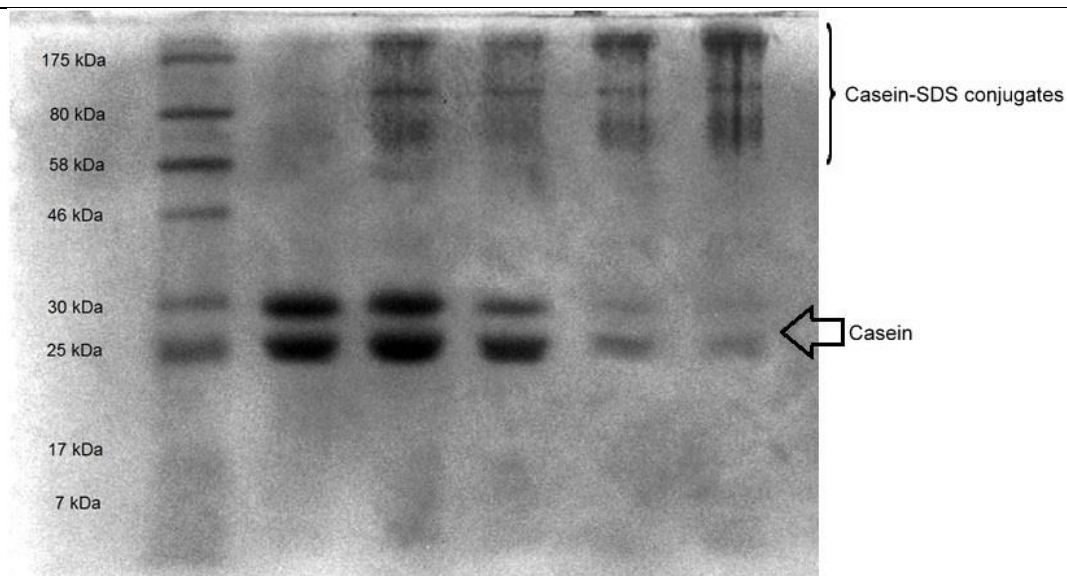


Figure 21: SDS-PAGE analysis of native Casein (lane 2), mixture of Casein and SDS after 12, 24, 36, and 48 of the Maillard reaction (lane 3–6) and pre-stained protein marker broad range, BioLabs (Lane 1). In each lane, 10 μ L of the sample with Casein concentration of 5mg/ mL⁻¹ was loaded.

7.2.3.3.1. Spectroscopic characterization of conjugates

Infrared spectroscopy is one of the oldest and well established experimental techniques for the analysis of secondary structure of polypeptides and protein. It can be used to establish the presence of protein-polysaccharide conjugation through Maillard reaction. The initial stage of this reaction has been sufficient for conjugation to be achieved between the protein and polysaccharide via the formation of covalent bond. During the reaction, an amide bond is formed through condensation between the amino group of amino acids (terminal and interstitial amines) or protein and the carbonyl group of reducing sugars.

From the FTIR results clear peak integration can be observed at 3700 and 1800 cm⁻¹ indicative of copolymerization of casein and SDS. However, nothing more significant can be categorized from the FTIR data. Larger characteristic peaks of absorption can be observed around 1650 characteristics of amine groups. A shift is visible in the 2200 cm⁻¹ region, characteristic of alkenes and alkynes. And a significant change is seen in the 1200 cm⁻¹ region characteristic of aliphatic amines. This might be a clear indication of protein polysaccharide interactions.

The amide band (1700-1600) cm⁻¹ arises almost entirely from the C=O stretching vibration of the peptide group. The amide band (1480-1575) cm⁻¹ is primarily N-H bending and a contribution from C-N stretching vibrations

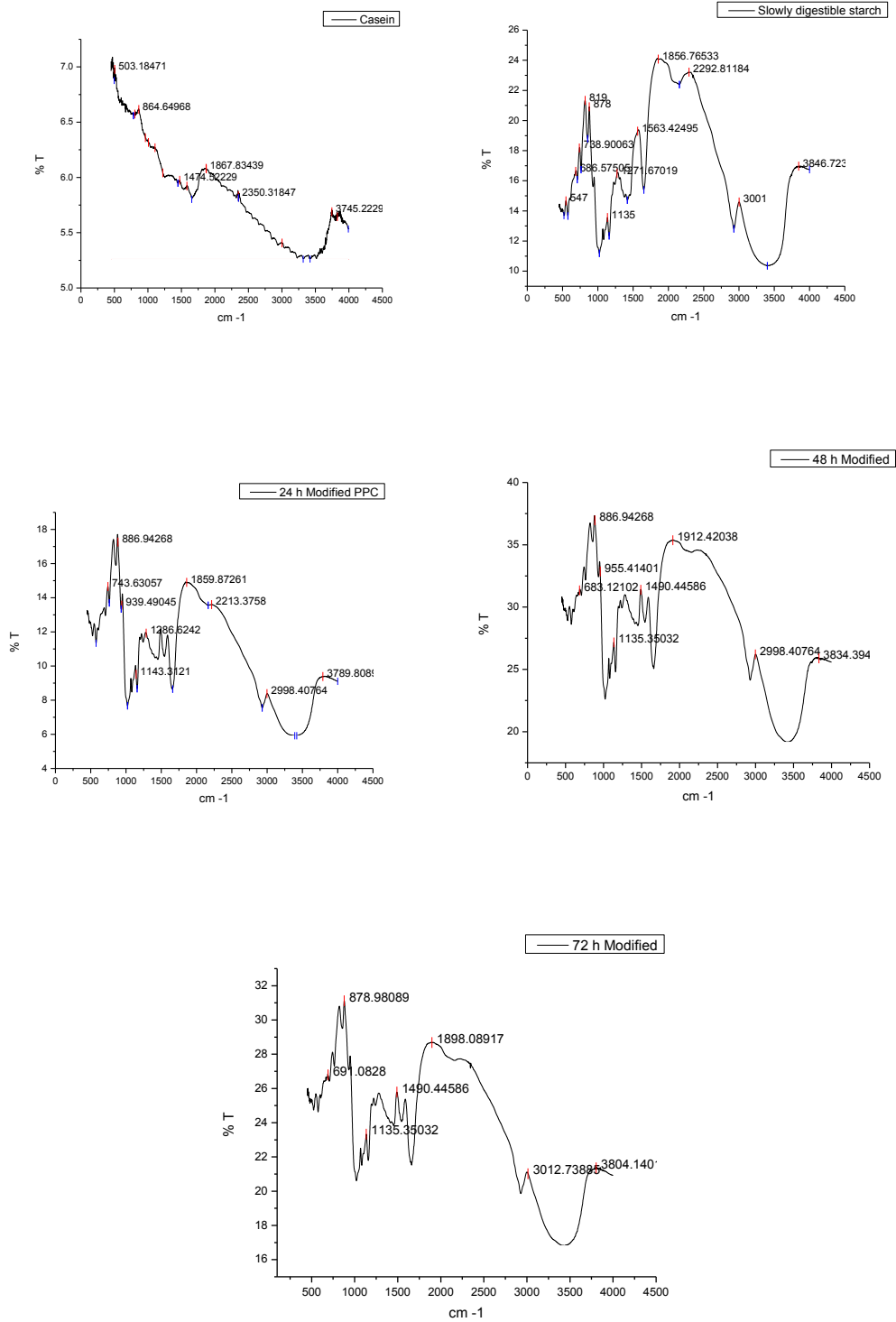


Figure 22: FTIR chromatograms from the top showing; Purified casein, SDS, 24 hour conjugate, 48 hour conjugate and 72 hour conjugate.

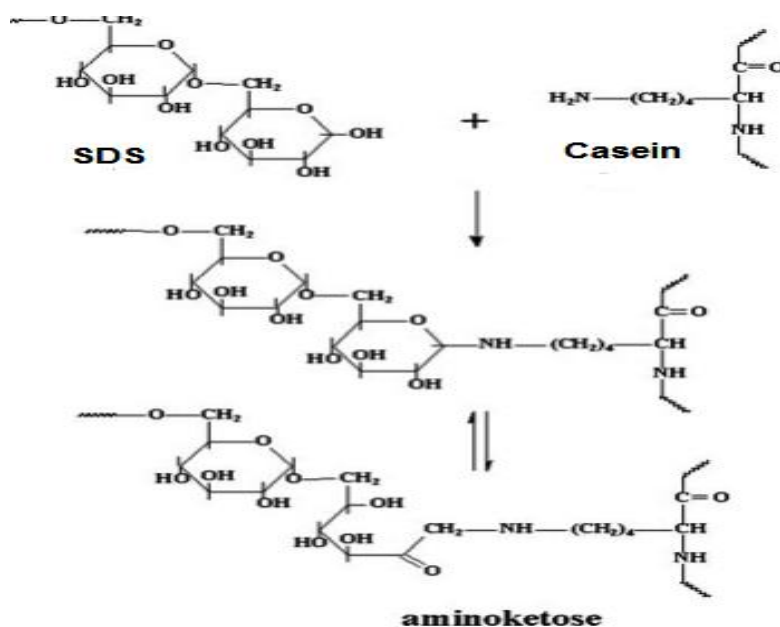


Figure 23: The structures of early stage products of casein-SDS Maillard reaction.

7.2.3.4. Surface characterization of nanocapsules and their dispersibility

The SEM images confirmed the formation of nanocapsules from the Casein-SDS conjugates. Both quercetin loaded and blank nanocapsules exhibited good structural integrity and spherical in shape.

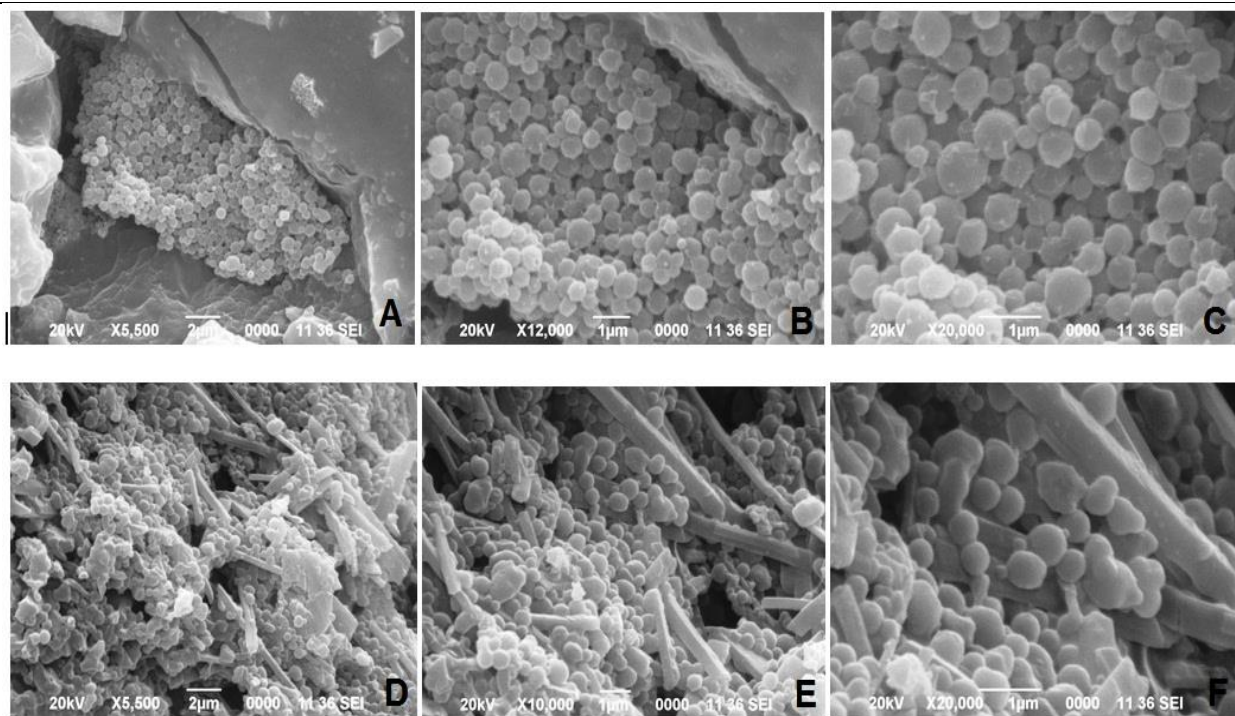


Figure 24: SEM image of Casein-SDS conjugate lyophilized nanocapsules at (A) 5,500x, (B) 12,000x (C) 20,000x and Quercetin loaded Casein-SDS conjugate lyophilized nanocapsules at (D) 5,500x, (E) 12,000x (F) 20,000x. The copolymer was prepared by Maillard reaction for 48 h with a molar ratio of casein to SDS of 1:1.

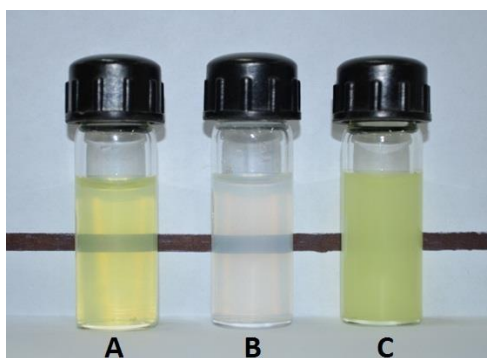


Figure 25: (A) Increased Solubility of Quercetin loaded nanocapsules (B) Solubility of Quercetin free nanocapsules (C) Compare to Free Quercetin in Water. It can be clearly visualized that Free Quercetin is Insoluble in Water.

The quercetin loaded nanocapsules were capable of solubilizing quercetin. As seen in figure 25, the quercetin loaded inside the nanocarriers in dispersed in the water medium; however, free quercetin at the same concentration does not dissolve readily in water. The nanocapsules were able to bind quercetin within the hydrophobic core of the particles and aid in dissolving quercetin.

7.2.3.4.1. Characterization of the Casein-SDS conjugates nanocapsules

The other most important study performed was the drug-interaction study of the drug and polymers. The presence of the peaks of the pure drug belonging to different functional group of the drug in the drug polymer mixtures confirms the stable nature of the drug in the drug-polymer mixture.

The FTIR spectra obtained from blank and quercetin loaded nanocapsules revealed few characteristic peaks of quercetin as shown previously in figure. However the blank quercetin lacked those peaks. The appearance of characteristic peaks of quercetin relation could be due to quercetin adsorbed to the surface of the nanocapsules.

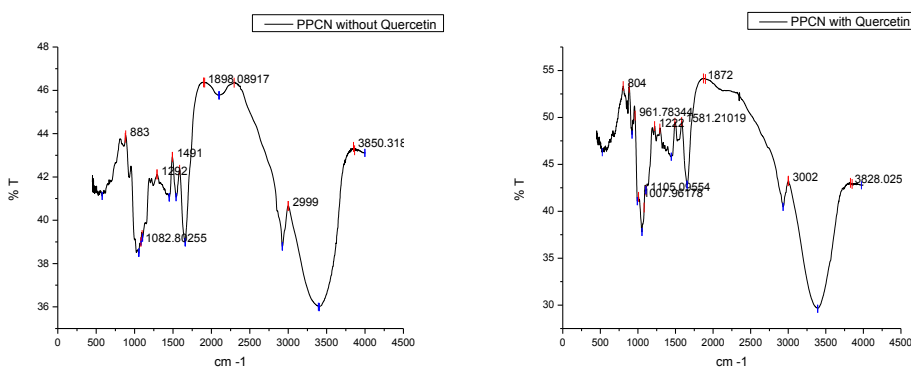


Figure 26: FTIR spectra of quercetin loaded and empty nanocapsules.

The spectra for free nanocapsules showed the characteristic bands of the polymer, $-\text{CH}$, $-\text{CH}_2$, $-\text{CH}_3$ stretching ($2850\text{--}3000\text{ cm}^{-1}$), carbonyl $-\text{C}=\text{O}$ stretching ($1700\text{--}1800\text{ cm}^{-1}$), $\text{C}-\text{O}$ stretching ($1050\text{--}1250\text{ cm}^{-1}$), and $-\text{OH}$ stretching ($3200\text{--}3600\text{ cm}^{-1}$). For quercetin, the spectra showed the characteristic bands corresponding to OH groups ($3700\text{--}300\text{ cm}^{-1}$), to $\text{C}=\text{O}$ absorption (1662 cm^{-1}), bands of $\text{C}-\text{C}$ stretching (1618 cm^{-1}), $\text{C}-\text{H}$ bending (1456 , 1383 , and 866 cm^{-1}), a band attributed to the $\text{C}-\text{O}$ stretching of the oxygen in the ring (1272 cm^{-1}), and the region for $\text{C}-\text{O}$ stretching ($1070\text{--}1150\text{ cm}^{-1}$). For pure quercetin, spectra exhibited the characteristic bands corresponding to OH stretching ($3600\text{--}3200\text{ cm}^{-1}$), $\text{C}=\text{C}$ stretching ($1600\text{--}1400\text{ cm}^{-1}$), $\text{O}-\text{H}$ stretching ($1800\text{--}1670\text{ cm}^{-1}$), $\text{C}-\text{O}$ stretching of the oxygen in the ring (1272 cm^{-1}), and the characteristic peaks for the disubstituted aromatic ring ($1200\text{--}900\text{ cm}^{-1}$). For quercetin-loaded nanocapsules, showed that the OH stretching band ($3200\text{--}3600\text{ cm}^{-1}$) is slightly shifted and increased in terms of energy absorption. These observations suggest that quercetin is associated with the polymer by hydrogen bonds. Also, in the quercetin-loaded nanocapsules, the band corresponding for $\text{C}=\text{O}$ stretching ($1700\text{--}1800\text{ cm}^{-1}$) was broader, indicating that quercetin is associated with the polymer by interactions between the carbonyl and the carboxyl groups of the flavonoid and the polymer. In addition, measurements confirmed the encapsulation of quercetin within the nanocapsules.

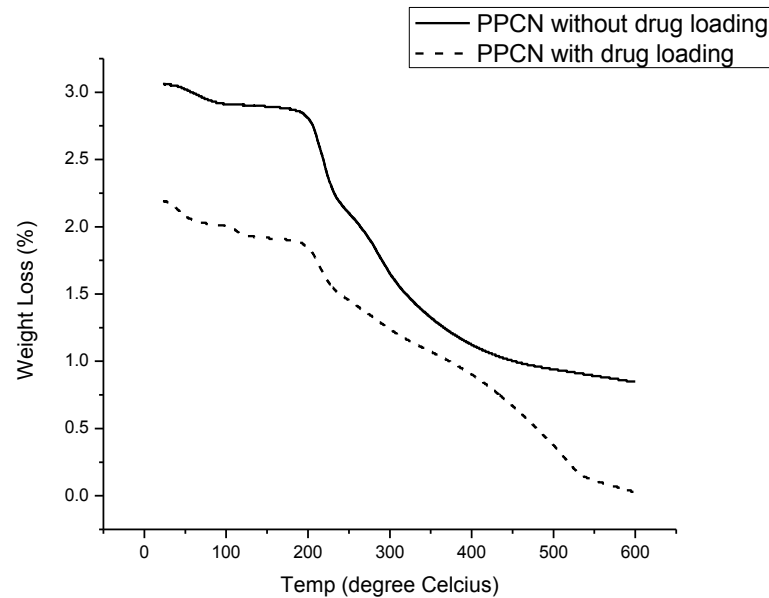


Figure 27: Thermo gravimetric analysis curves of nanocapsules with and without drug loading.

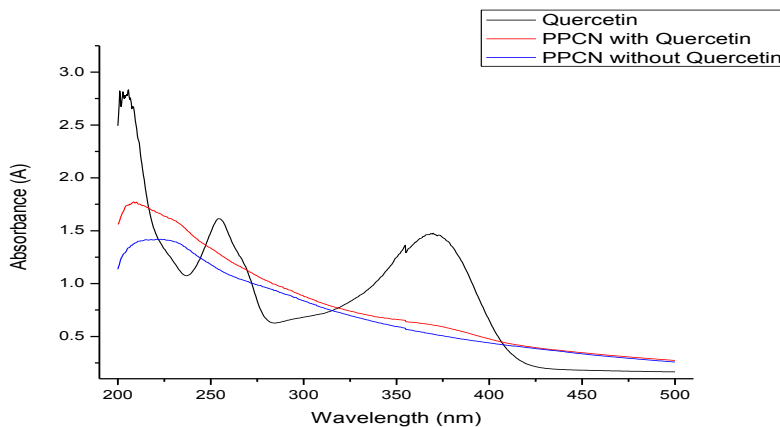


Figure 28: UV-Visible Spectra of Quercetin, nanocapsules without Quercetin and nanocapsules with Quercetin loaded.

The TGA thermograms (Figure 27) showed a gradual decline in the weight of the capsules. However, the drug loaded nanocapsules looked more stable as weight was more gradual, than compared to the blank nanocapsules. The initial gradual loss of weight could be attributed to loss of bound and free moisture content. However after 180-200°C, a much rapid and weight loss of weight was seen in the blank nanocapsules. This might be due to degradation of SDS and casein. At higher temperatures proteins are known to unfold and degrade and this went consistent with known findings from literature.

The UV-VIS reading (Figure 28) showed two characteristic absorbance peaks of Quercetin at 254nm and 386nm. However, the drug loaded and blank nanocapsules lacked these peaks. The lack of this characteristic absorbance in the drug loaded nanocapsules suggested efficient drug loading. And drug loading efficiency as determined from the dialysis experiment confirmed 86% drug loading efficiency of these nanocapsules.

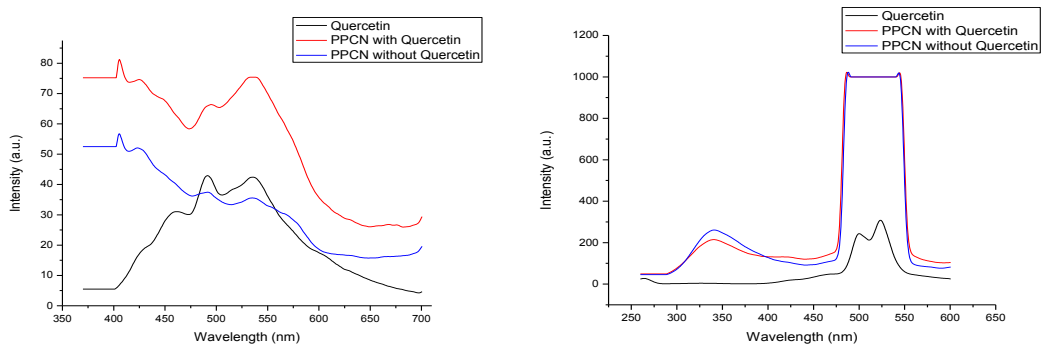


Figure 29: Fluorescence spectra of Quercetin, loaded and blank nanocapsules at 254nm and 368nm.

Fluorescence spectroscopic emission (Figure 29) was observed against excitation at 368nm and 254nm. At 368nm, characteristic emission of quercetin fluorescence was observed, however, such emissions were not observed in quercetin loaded and blank nanocapsules, indicating proper encapsulation. However, slight fluorescence was observed in the quercetin loaded nanocapsules, and this might be explained as fluorescence of quercetin adsorbed at the surface of the loaded nanocapsules.

However, at 254nm, fluorescence from the quercetin and blank Nanocapsules could not be observed due to Raman scattering, which was same for the analyte fluorescence and the solvent scattering.

7.2.3.4.2. Characterization of the nanocapsules size and zeta potential

Size estimation of nanocapsules using image analysis techniques in SEM, revealed an average size of 450 nm for both the types of nanocapsules produced. However, DLS experiments (Figure 30) were conducted by hydrating nanocapsules in an aqueous medium. This revealed an increase in size of the Nanocapsules. The blank nanocapsules were measured at average 957 nm and the loaded nanocapsules were measured at average 897 nm respectively.

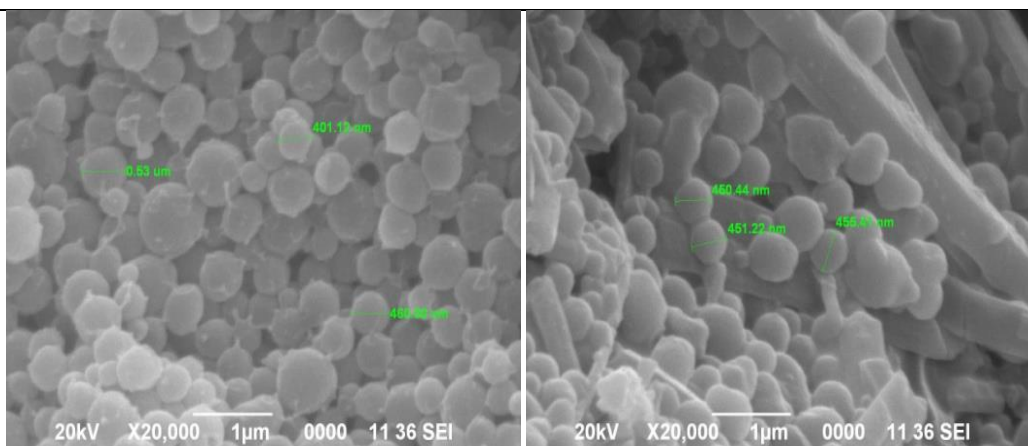


Fig 30: Size estimation of lyophilized quercetin loaded and without quercetin loading nanocapsules

The increase in size of the Nanocapsules when hydrated could be due the fact that SDS is highly hygroscopic. However, interestingly the quercetin loaded nanocapsules were relatively more compact in the aqueous medium at neutral pH. This could be due to the formation of bond interactions between quercetin and the casein protein. The increased bond formation could have stabilized the protein further and led to a more compact structure than the empty nanocapsules.

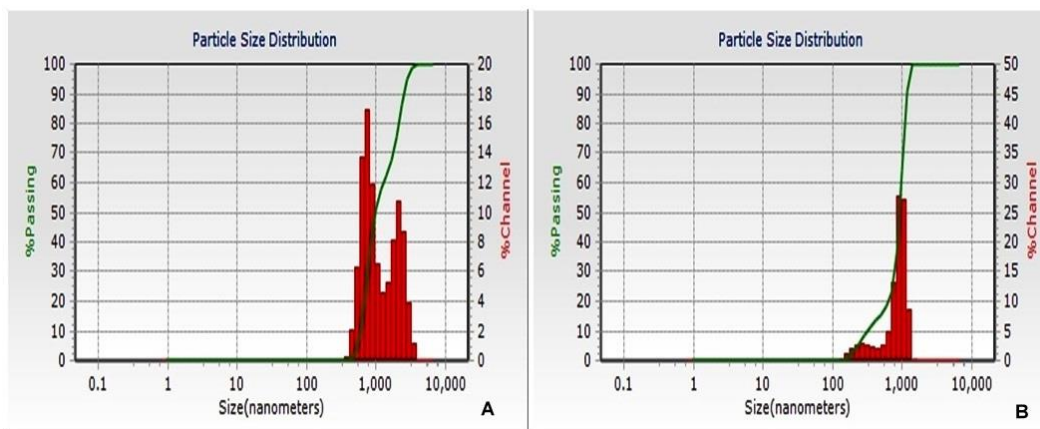


Figure 31: Scattering light intensity of (A) casein-SDS conjugate nanocapsules, (B) quercetin loaded casein-SDS conjugate nanocapsules at neutral pH. The conjugate polymer was prepared by Maillard reaction for 48 h with a ratio of casein to SDS of 1:1 (w/w).

The diluted samples at pH 7.0 were also measured for zeta-potential. Blank and Loaded nanocapsules showed a zeta potential of -2.5mV and -1.9 mV respectively at pH 7. A zeta potential away from neutral is preferable, as this leads to nanocapsule stability in solutions and

self aggregation and assembly is avoided.

7.2.3.4.3. pH regulated drug release characteristics of the nanocapsules under *in vitro* conditions

Encapsulation capacity of quercetin within the nanocapsules was found to be $76\pm 4\%$. Quercetin loaded nanocapsules showed sustained release behaviors of quercetin from within the hydrophobic core. During simulated gastric digestion the release profile was almost stagnant due to the protective coating provided by SDS, and also due to the fact that casein micelles are very compact near its pI.

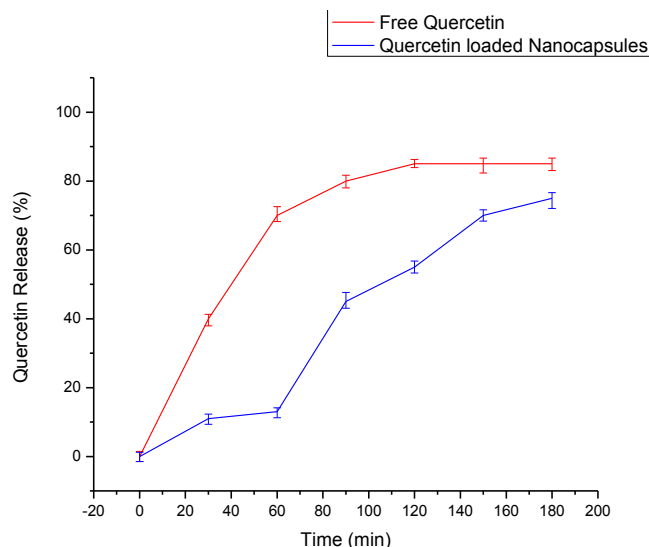


Figure 32: Quercetin release from nanocapsules under simulated gastric and intestinal digestion.

However, after that change of pH into intestinal conditions, there was an abrupt release of quercetin, which might be due to loosening of the casein structure at pH close to neutral. After this period a sustained release was observed. The data was compared to release of free quercetin and, free quercetin seemed to readily cross the membrane within the first 60 to 80 minutes.

The drug release from the nanocapsules was compared to a control of free quercetin release from the dialysis bag to give a clear indication of drug release.

7.2.4. *In silico* studies of biomolecule binding with nanocapsule

7.2.4.1. Modeling of b-casein

The model of casein micelle as proposed by Dalglesih, 2011 suggests that b-casein forms the inner core of a casein micelle. Therefore, it was hypothesized that b-casein will form the inner core of the polymeric Nanocapsules too. B-Casein micelle structure was modeled using I-TASSER web based server (Roy et al., 2010), which is a protein structure modeling approach based on the secondary- structure enhanced profile–profile threading alignment (PPA) and the iterative implementation of the Threading Assembly Refinement (iTASSER) program.

The b-casein molecule was modeled using the web based iTASSER server, and model predicted by it showed good protein modeling characteristics. From the ramachandran plot shown in figure, it is evident the most of the phi and psi angles lie in the favorable region. The ramachandran plot was generated using Discovery studio visualize client 4.0. It is characteristic of good protein models that the phi and psi angle lie in the favorable region as shown in the ramachandran plot diagram.

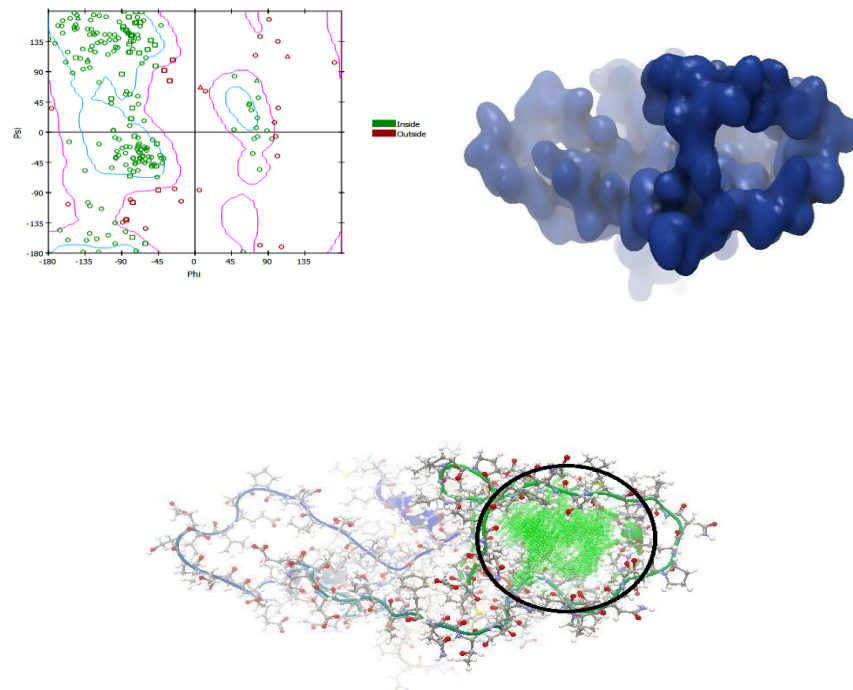


Figure 33: From the top, Ramachandran plot showing the distribution of phi-psi angles of modeled b-casein,

surface view of modeled b-casein and quercetin binding site cavity of b-casein as predicted by CLC Workbench.

7.2.4.2. Docking of quercetin to b-casein

As shown in figure 33, the docking region highlighted in green was taken as the docking site cavity from b-casein. This region was predicted by the CLC workbench inbuilt docking cavity search program.

From the figure it is evident that quercetin has formed active docking with b casein. And from overlapping images it is evident that the formation of these additional bonds with the bcasein molecule has resulted in a more stable confirmation of the structure.

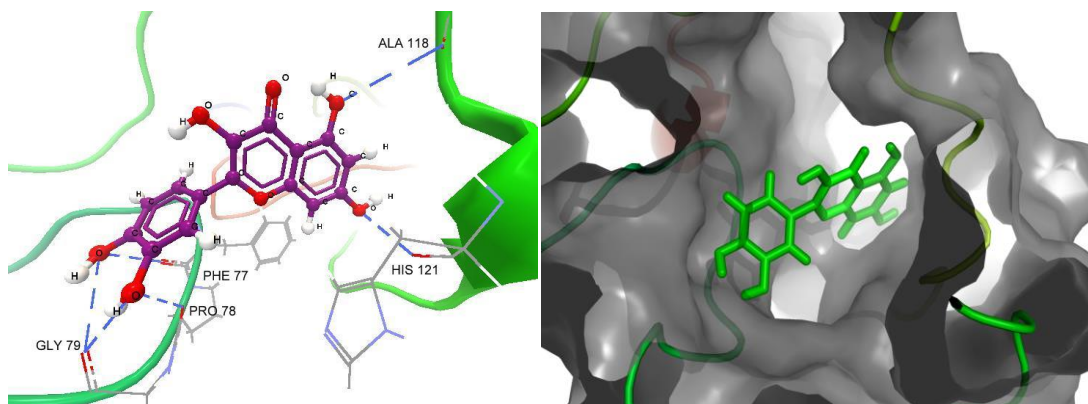


Figure 34: Showing the interaction of quercetin in the binding site cavity of the b casein protein.

7.2.4.3. Molecular dynamic simulation studies

MD simulation was run for a period of 10 ns, and the trajectories were stable during the whole production part of the 10,000-ps MD simulation run. The trajectory stability was checked and corroborated by the analysis of the root mean square deviation (RMSD) (Fig. 36) as functions of time for b-casein and its complexes with quercetin. The analysis of Fig. 43a indicates that the RMSD of protein systems reached equilibrium and oscillated around the average value after about 6000-ps simulation time. This evidence clearly indicates that the system was stable and equilibrated.

In the present MD study, the radius of gyration (R_g) values of quercetin and b-casein–quercetin complexes were determined and plotted as a function of time, as shown in Fig. 43a. In the protein systems, the R_g values kept dropping, indication a decrease in the hydrodynamic diameter of the protein molecule.

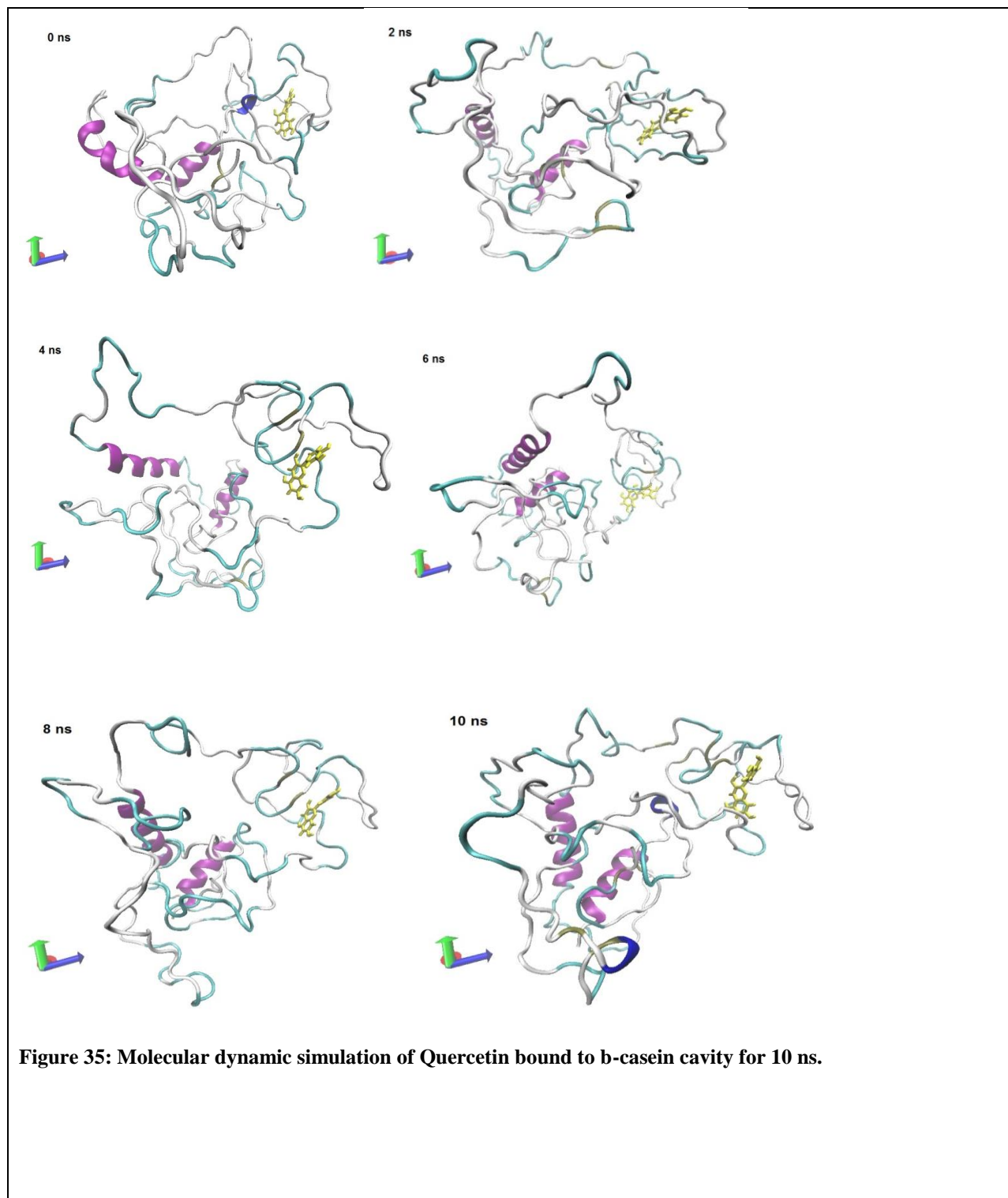


Figure 35: Molecular dynamic simulation of Quercetin bound to b-casein cavity for 10 ns.

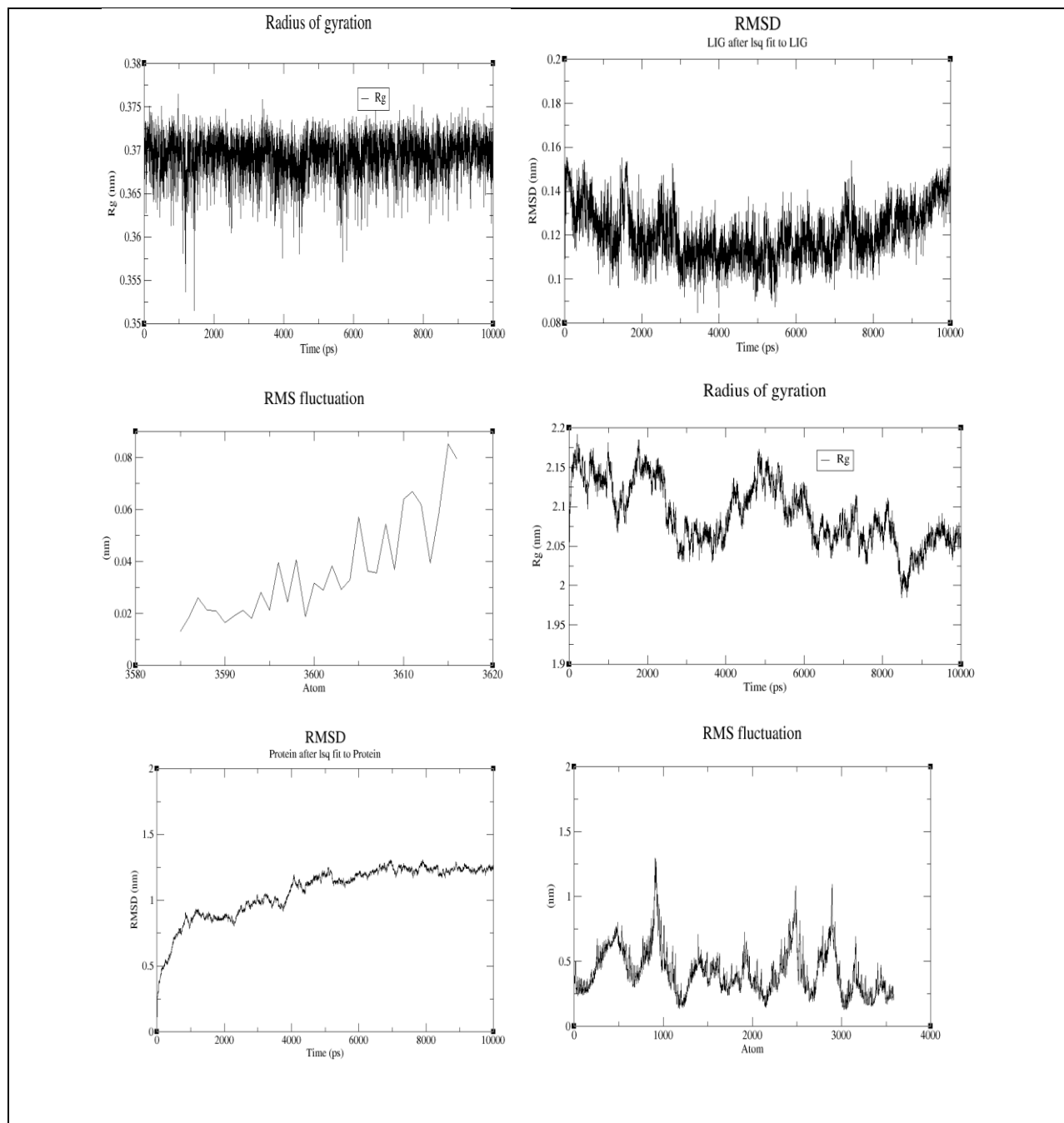


Figure 36: GROMACS dynamic analysis plots from the top; radius of gyration of Ligand, Ligand RMSD, Ligand RMSF, radius of gyration of bcasein, bcasein RMSD, bcasein RMSF.

Local protein mobility was analyzed by calculating the time-averaged root mean square fluctuation (RMSF) values of b-casein–quercetin complexes. The results were plotted against residue numbers based on 10,000-ps trajectory (Fig. 36). Also, the structure of ligand binding site remained approximately rigid during simulation.

Docking calculations showed the probable binding site of quercetin is located in the hydrophobic core of b-casein where the quercetin molecule is lined by hydrophobic residues and make five hydrogen bonds and several van der Waals contacts with them. Moreover, molecular dynamic (MD) simulation results suggested that this flavonoid can interact with b-casein, without affecting the secondary structure of b-casein. Simulations, molecular docking and experimental data reciprocally supported each other.

7.3 Innovations:

- ✓ Target ADAM17 has been exploited to inhibit the cascade of cytokine signaling particularly TNF alpha and thereby hoping to stop the over expression of the NFkB pathway. ADAM17 can be a key target for control of inflammatory bowel disease control. After screening of known compounds that provide relief in inflammatory bowel disease models, quercetin has come as the molecule that is most effective against the ADAM 17 metalloproteinase in terms of target binding, interaction with active site residue GLU406, pharmacokinetic parameters and dynamic simulation in a water environment.
- ✓ Optimization levels for solvent, time, concentration of acid for extraction of quercetin were found to be solvent concentration= 74.38%, irradiation time= 5.09 minutes and acidification was 1.75% respectively. The predicted extraction yield of quercetin was 0.31 mg/gm, which was consistent with the practical extraction yield of quercetin of 0.29 mg/gm.
- ✓ Casein-SDS nanocapsules were prepared and drug loading efficiency of 76% was observed. The nanocapsules demonstrated sustained release profiles of quercetin. Loaded and black nanocapsules (lyophilized powder) had a mean diameter of 450nm.
- ✓ Nanocapsule characterization of quercetin release behavior indicated a pH responsive release behavior. After initial SDS coat digestion at acidic gastric pH, the nanocapsules showed a higher degree of drug release in the nearly neutral pH of the intestine.

7.4 Application Potential:

7.4.1 Long Term:

Inflammatory bowel disease is an auto immune disease that is caused by several environmental and genetic factors. Current strategies to contain the disease have attained considerable success with monoclonal antibody therapy. However, these strategies are very expensive. In countries like India, where a large chunk of the population live below the poverty line, or fall in the lower middle class will not be able to afford these medications.

Our understanding of the pathogenesis of diseases alongside with therapeutic polyphenolic molecules has advanced enormously in recent decades. As a consequence, drug discovery has gradually shifted from an entirely human phenotype-based endeavor to today's reductionist approach centered on single molecular targets. Clearly, other information has to be exploited as effectively as possible, in terms of targeted delivery of these biomolecules to the disease area.

Biomolecules that are very poorly stable need to be protected in their passage through the gut environment in suitable nano/micro carriers that will ensure their protection from degradation and ensure bioavailability. Therefore effective encapsulation strategies are needed to promote targeted delivery, polyphenol stability, absorption and bioavailability during its journey to the colon. Nanocapsules have shown to promote targeted delivery, polyphenol stability, absorption and bioavailability. Slow drug release profiles of encapsulating coat are necessary to promote bioavailability in the colon. This dissertation, has suggested a new approach of target identification, biomolecule screening against particular identified targets, development of nanocarrier system meeting the necessity for the job, and incorporation in food matrix for oral

consumption. This approach can help to design Low cost Biofunctional foods that might help to provide therapeutic benefit in inflammatory bowel disease. The new approach will ensure higher accuracy in Biofunctional food based therapies.

7.4.2 Immediate

The present work for the first time, describes a novel process to enrich quercetin in crude Bhut jolokiya (a Capsicum chinense Jacq. cultivar) extract by using a simultaneous microwave assisted acid hydrolysis process for sample preparation, followed by downstream purification of quercetin using SPME and HPLC. In particular, the developed process incremented the separation and purification of pure quercetin by ~3.75 folds in comparison to conventional microwave assisted extraction. The findings of this study can contribute as a guide for future research in the area of combinatorial extraction techniques and separation of pure molecules from glycoside conjugates. Additionally, the literature can contribute towards future scale-up studies for industry-scale isolation and purification of quercetin by food and pharmaceutical industries.

ADAM17 is an attractive target for the development of new anti-inflammatory drugs. We aimed to identify selective inhibitors of ADAM17 against matrix metalloproteinase enzymes (MMP-1, MMP-2, MMP-3, MMP-7, MMP-8, MMP-9, MMP-13, and MMP-16) which have substantial structural similarity. Target proteins were docked with natural molecule ligands and a known selective inhibitor IK682. Quercetin was the most selective inhibitor of ADAM17.

7.5 Any other -

8. Research work which remains to be done under the project (for on-going projects)

- Work on studying profile of marker expression in cell line model against biomolecule
- and Incorporating Nanocomposites in a suitable food/dairy matrix as a carrying vehicle.

Ph.Ds Produced no: 01 (on-going)

Technical Personnel trained: 02

Research Publications arising out of the present project: 02 (communicated)

List of Publications from this Project (including title, author(s), journals & year(s))

(A) Papers published only in cited Journals (SCI)

- i). Pallab Kumar Borah, Sankar Chandra Deka, Raj Kumar Duary. Effect of repeated cycled crystallization on digestibility and molecular structure of glutinous rice starch. *International Journal of Biological Macromolecule*. (Under Revision)
- ii). Pallab Kumar Borah, Nikhil Kumar Mahnot, Anindhya Sundar Das, Anandita Basu, Dipankar Kalita, Rupak Mukhopadhyay, Raj Kumar Duary. Enhancing the separation of quercetin in Bhut jolokiya: Simultaneous microwave assisted acid hydrolysis process, structure identification and anti-inflammatory property. *Separation Science and Technology* (Under review).

(B) Papers published in Conference Proceedings, Popular Journals etc.

- i). Lopamudra Sarma, Preeti Sarkar and Raj Kumar Duary. 2015. *In silico* inhibition studies of various fruits and medicinal plant derived polyphenol against nuclear factor NF-kB pathway (p50 subunit) expressed during pro-inflammatory signaling pathway. National conference cum workshop organizing organized by the Food Engineering and Technology Dept, Tezpur University, 27 to 28th March, 2015 on Innovative prospects in food processing: integration of engineering and biological sciences.

Patents filed/ to be filed:

Borah, P.K., Duary, R.K. 2016. Slow Digestible Starch Casein nanoparticle for colon targeted controlled delivery of biologically active agents in food systems. (Provisional Application No. 201631005351 (E-2/285/2016-KOL).

Major Equipment (Model and Make)					
S No	Sanctioned List	Procured (Yes/ No) Model & make	Cost (Rs in lakhs)	Working (Yes/ No)	Utilisation Rate (%)
1	Refrigerator	Yes GL-M- 322RLTL (NS); LG	0.35	Yes	100
2	Digital Analytical Balance	ME204; METTLER TOLRADO	2.65	Yes	100
3	Table top lab Drying Oven	1210D/10; JSGW		Yes	100
4	pH meter	PH700; EUTECH		Yes	100
5	Table top laboratory digital water bath	1210; JSGW		Yes	100

Raj Suany

UTILIZATION CERTIFICATE

[FOR THE FINANCIAL YEAR 2016-2017 (01.04.2016 to 31.03.2017)]

1. Title of the Project/Scheme: **Encapsulation and controlled delivery of herbal extracts in diary food matrix using cow milk protein against in vitro simulated inflammatory cell line models. (Under Start-Up Research Grant (Young Scientists)-Life Science)**
2. Name of the Institution: **Tezpur University**
3. Name of the Principal Investigator: **Dr. Raj Kumar Duary**
4. Science and Engineering Research Board (SERB)
Sanction order No & date sanctioning the project:
(First financial sanction order) **SB/YS/LS-30/2014 dated 10 October, 2014**
5. Head of account as given in the original sanction order:

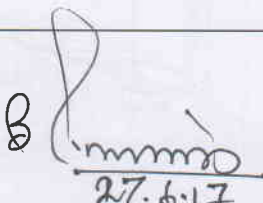
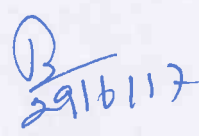
Head	Amount
Non-recurring (Equipments)	₹ 3,00,000
Recurring (Manpower, Consumables, Travel, Contingencies, Overhead)	₹ 16,70,000

6. Amount brought forward from the previous Financial year quoting SERB letter no and date in which the authority to carry forward the said amount was given
i. Amount: - ₹ 10, 475.00 (minus)
ii. SB/YS/LS-30/2014
iii. Date: 24.08.2016
7. Amount received during the financial year (SERB Sanction order no and date)
i. Amount: ₹ 6,00,000
ii. Order No: SB/YS/LS-30/2014
iii. Date: 24.08.2016
8. Total amount that was available for expenditure (excluding commitments) during the financial year (Sr. No. 6 + 7) **₹ 5,89,525.00**
9. Actual Expenditure (excluding commitment): **₹ 5,89,600.00**
10. Balance amount available at the end of the financial year:(-) **₹ 75.00 (minus)**
11. Unspent balance refunded, if any (details of cheque no. etc): NIL
12. Amount to be carried forward to the next financial year: Nil


Assistant Professor
Deptt. of Food Engineering & Technology
Tezpur University, Napaam-784028
Dist-Sonitpur (Assam)

UTILIZATION CERTIFICATE

Certified that out of ₹ 6,00,000.00 of grants-in-aid sanctioned during the year 2016-2017 in favour of Tezpur University vide SERB order No. SB/YS/LS-30/2014 dated 24/08/2016 and ₹ (-) 10,475.00 (minus) on account of unspent balance of the previous year, a sum of ₹ 5,89,600.00 has been utilised for the purpose of project entitled "Encapsulation and controlled delivery of herbal extracts in dairy food matrix using cow milk protein against in vitro simulated inflammatory cell line models." for which it was sanctioned and that the balance of Rs. (-) 75.00 (minus) remaining unutilized at the end of the year will be adjusted towards the grants-in-aid payable during the next year *i.e.* 2017-2018.

 Signature of PI: Date: <u>16/06/2017</u>	 Signature of the Finance Officer: Date: <u>27.6.17</u> <i>Finance Officer</i> <i>Tezpur University</i>	 Signature of the Registrar: Date: <u>29/6/17</u> <i>Registrar</i> <i>Tezpur University</i>
--	---	--

Assistant Professor
Dept. of Food Engineering & Technology
Tezpur University, Napaam-784026
Dist. Sonitpur (Assam)

REQUEST FOR ANNUAL INSTALMENT WITH UP-TO-DATE STATEMENT OF EXPENDITURE

1. SERB Sanction Order No and date : SB/YS/LS-30/2014 dated 10 October, 2014
 2. Name of the PI : Dr. RAJ KUMAR DUARY
 3. Total Project Cost : Rs. 19,70,000.00
 4. Revised Project Cost : NA
 5. Date of Commencement : October 10, 2014
 6. Statement of Expenditure
 (month wise expenditure incurred during current financial year April, 2016 to March, 2017)

Month & year	Expenditure incurred (Rs.)
April, 2016	
May, 2016	
June, 2016	
July, 2016	
August, 2016	
September, 2016	13,904.00
October, 2016	1,34,500.00
November, 2016	(include JRF scholarship from April, 2016 to September 2016) 12,000.00
December, 2016	12,000.00
January, 2017	12,000.00
February, 2017	3,63,660.00
March, 2017	41,536.00

7. Grant received in each year
 a. 1st Year : Rs. 7,00,000.00
 b. 2nd Year : Rs. 3,00,000.00
 c. 3rd Year : Rs. 6,00,000.00
 d. Interest, if any: NIL
 e. Total (a+b+c+d): Rs. 16,00,000.00


 Assistant Professor
 Deptt. of Food Engineering & Technology
 Tezpur University, Napaam-784028
 Dist-Sonitpur (Assam)

Statement of Expenditure1st April 2016 to 31st March 2017

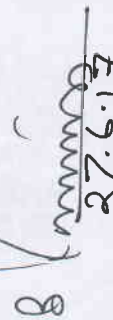
Sr No (I)	Sanctioned Heads (II)	Total Fund Received (2014-15) & (2015-16) & (2016-17) (III) In ₹	Expenditure Incurred			Total Expenditure till 31 st March 2017 (VII = IV + V + VI) In ₹	Balance as on 31 st March 2017 (VIII = III - VII) In ₹	Requirement of Funds upto 31 st March 2018 In ₹	Remarks (if any)
			1 st Year 2014-15 (IV) In ₹	2 nd Year 2015-16 (V)	3 rd Year 2016-17 (VI)				
1.	Manpower costs	3,41,600.00	65,600.00	1,44,000.00	1,32,000.00	3,41,600.00	0.00	72,000.00	
2.	Consumables	7,56,996.00	0	3,75,875.00	3,81,1956.00	7,57,071.00	- 75.00	2,18,000.00	
3.	Travel	13,904.00	NIL	NIL	13,904.00	13,904.00	0	40,000.00	
4.	Contingencies	NIL	NIL	N/A	N/A	0	0	10,000.00	
5.	Others (Tax)	NIL	NIL	N/A	N/A	NIL	NIL	NIL	
6.	Equipment	3,00,000.00	35,000.00	2,65,000.00	N/A	3,00,000.00	0.00	0.00	
7.	Overhead	1,87,500.00	62,500.00	62,500.00	62,500.00	1,87,500.00	0.00	0.00	
8.	Total	16,00,000.00	1,63,100.00	8,47,375.00	5,89,600.00	16,00,075.00	- 75.00	3,40,000.00	

Name of Principal Investigator: Dr. RAJ KUMAR DUARY



Signature of PI:

Date: 16/06/2017

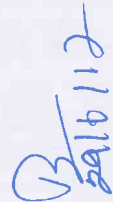


Signature of the Finance Officer:

Date:

Finance Officer

Tezpur University



Signature of the Registrar:

Date:

Registrar

Tezpur University

Assistant Professor

Dept. of Food Engineering & Technology

Tezpur University, Napaam-784028

Dist-Sonitpur (Assam)